CKDMIP: CKD tool performance evaluation

May 3, 2020

CKD tool: **ecCKD version 0.5**
Spectral domain: **Longwave**
Application: **Global NWP**
Evaluation dataset: **Evaluation-1**

Contents

Overview

This automatically generated document contains an evaluation of the performance of ecCKD for generating longave correlated k-distribution (CKD) gas-optics models targeting the application *Global NWP*: atmospheric heating rates are required to a minimum pressure of 0.02 hPa, and evaluation is performed for present-day greenhouse gas concentrations. The evaluation dataset is *Evaluation-1* from the Correlated K-Distribution Model Intercomparison Project (CKDMIP)[1]. Longwave radiative transfer is performed using four angles per hemisphere.

[1] `https://confluence.ecmwf.int/display/CKDMIP`

The ecCKD tool has been used to generate CKD models with the following band structure(s): *fsck* (one full-spectrum band), *wide* (5 bands) and *narrow* (13 bands). For each band structure, a number of CKD models have been generated, characterized by the total number of k terms (also known as g points).

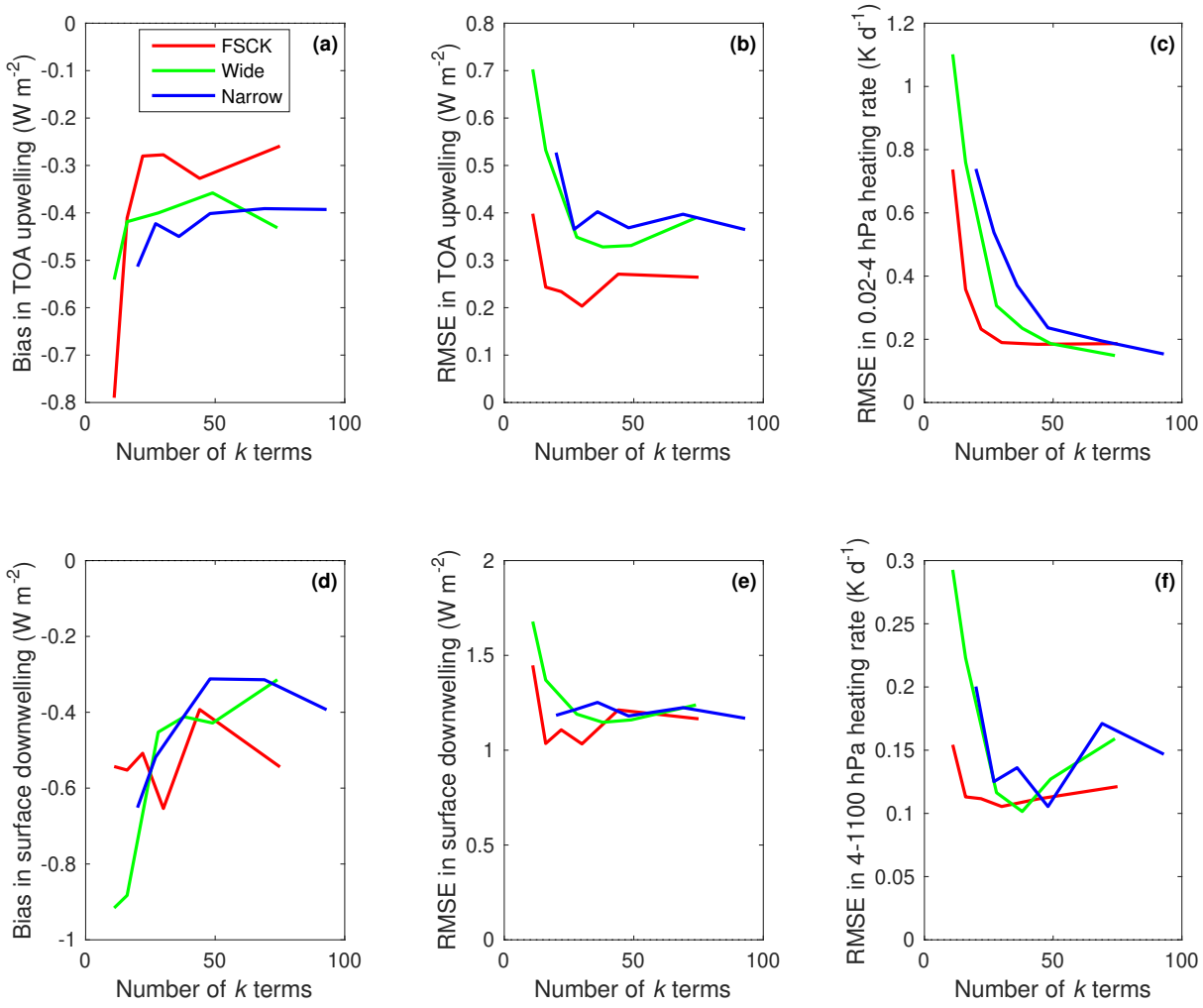

Biases and root-mean-squared errors (RMSE) in top-of-atmosphere (TOA) upwelling irradiance and surface downwelling irradiance, and RMSE in heating rate for two pressure ranges, for the various band structures as a function of the total number of k terms. It was computed from the "present-day" CKDMIP scenario.

Model 1: ecCKD global-nwp-fsck-11

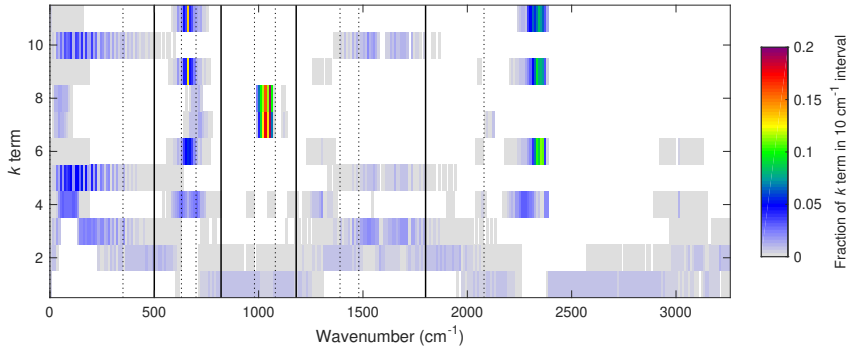

Illustration of the parts of the longwave spectrum that contribute to each k term of the global-nwp-fsck-11 model.

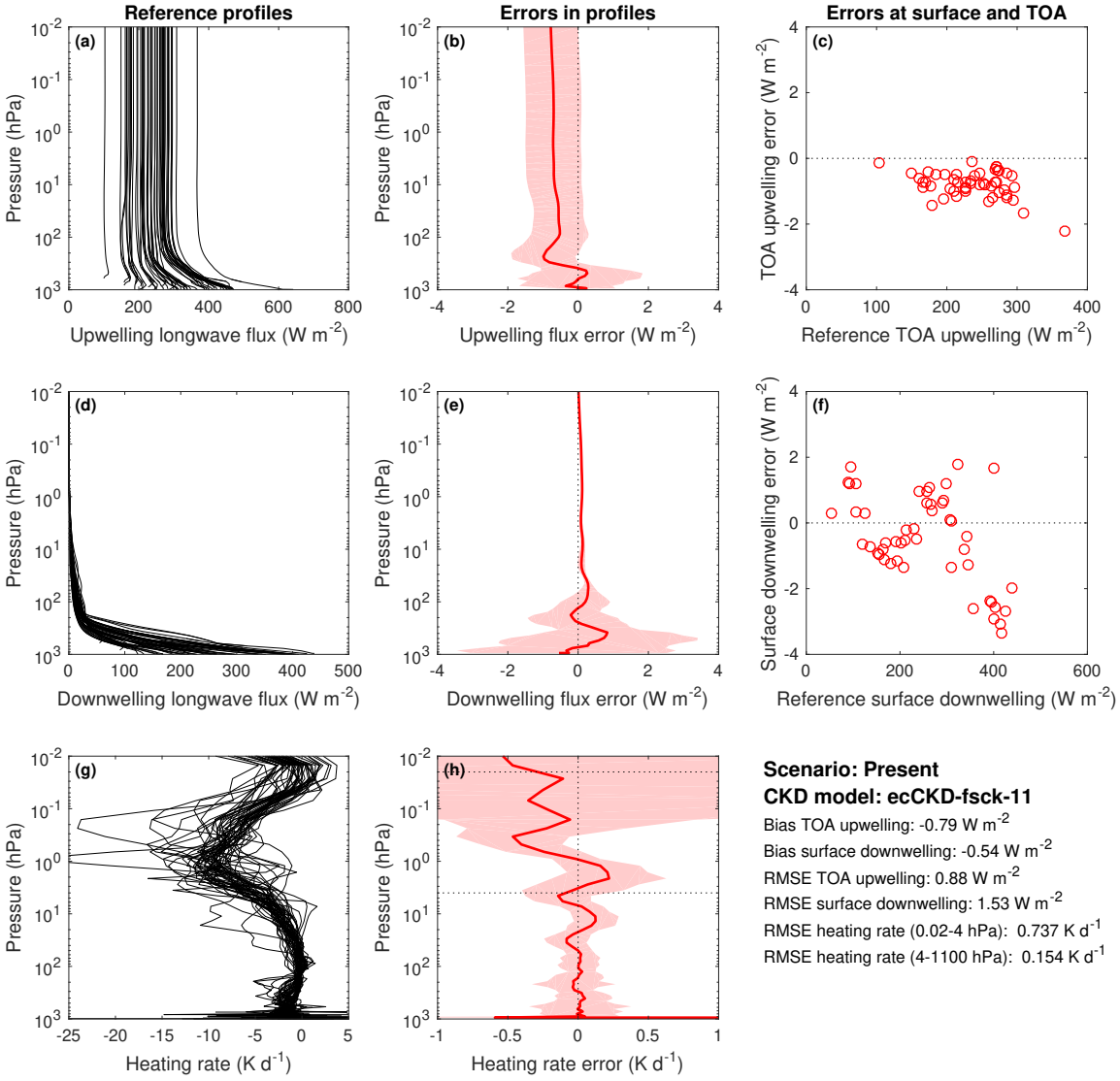

Evaluation of the global-nwp-fsck-11 CKD model for the "present-day" CKDMIP scenario. The left three panels show the irradiances and heating rates from the reference line-by-line calculations. The red lines in the middle three panels show the corresponding bias in these quantities from the CKD model. The shaded regions encompass 95% of the instantaneous errors. Panels c and f depict instantaneous errors in upwelling TOA and downwelling surface irradiances. Error metrics are provided in the lower right.

Model 2: ecCKD global-nwp-fsck-16

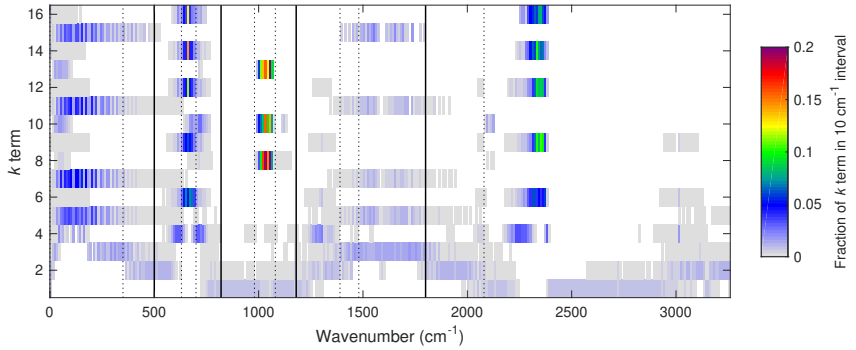

Illustration of the parts of the longwave spectrum that contribute to each k term of the global-nwp-fsck-16 model.

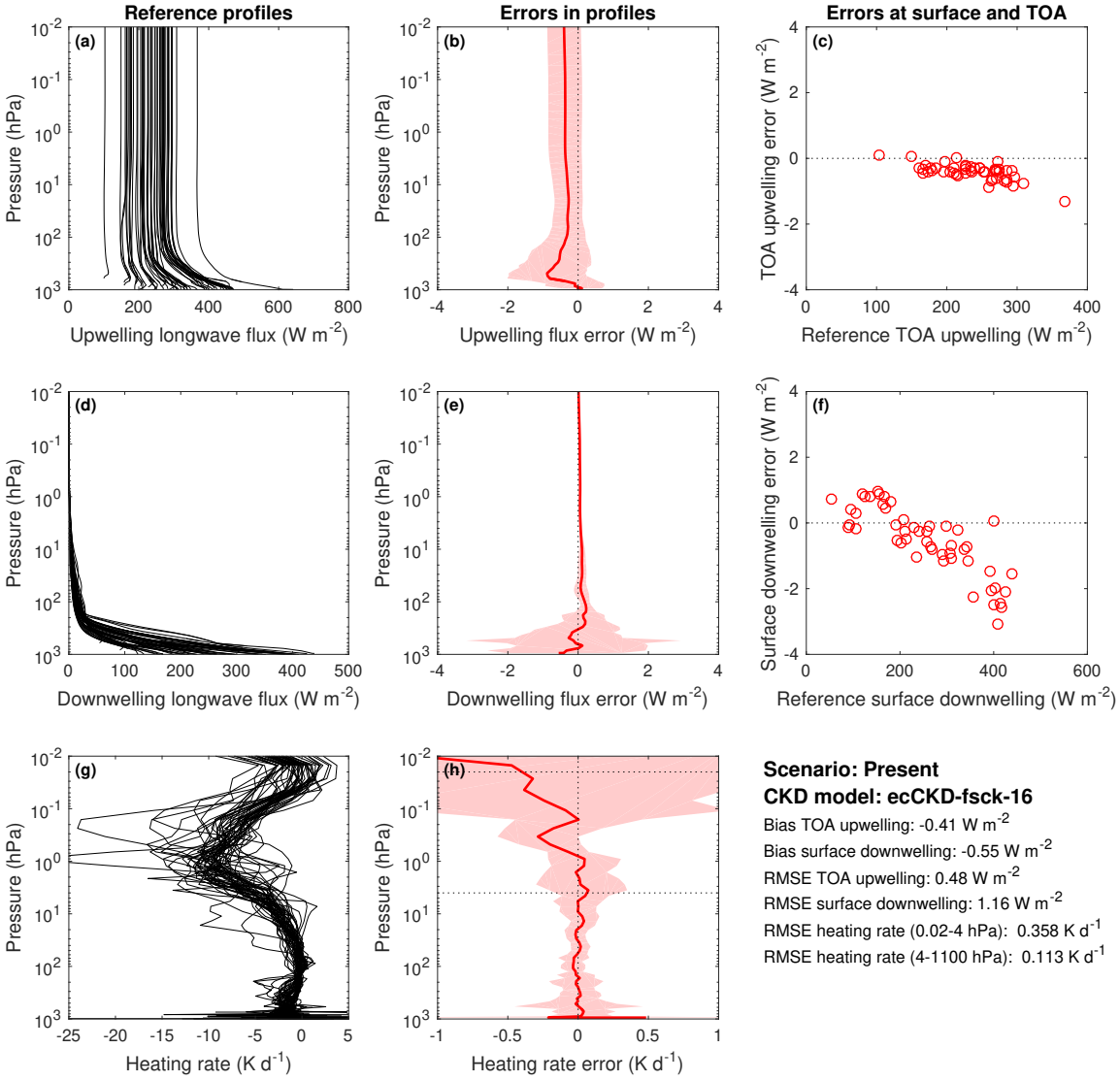

Evaluation of the global-nwp-fsck-16 CKD model for the "present-day" CKDMIP scenario. The left three panels show the irradiances and heating rates from the reference line-by-line calculations. The red lines in the middle three panels show the corresponding bias in these quantities from the CKD model. The shaded regions encompass 95% of the instantaneous errors. Panels c and f depict instantaneous errors in upwelling TOA and downwelling surface irradiances. Error metrics are provided in the lower right.

Model 3: ecCKD global-nwp-fsck-22

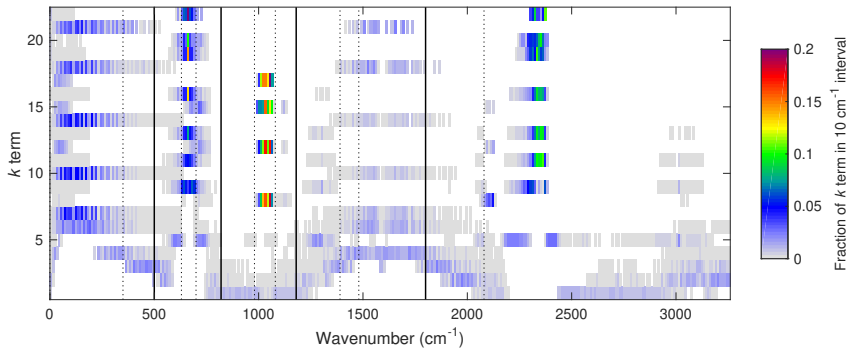

Illustration of the parts of the longwave spectrum that contribute to each k term of the global-nwp-fsck-22 model.

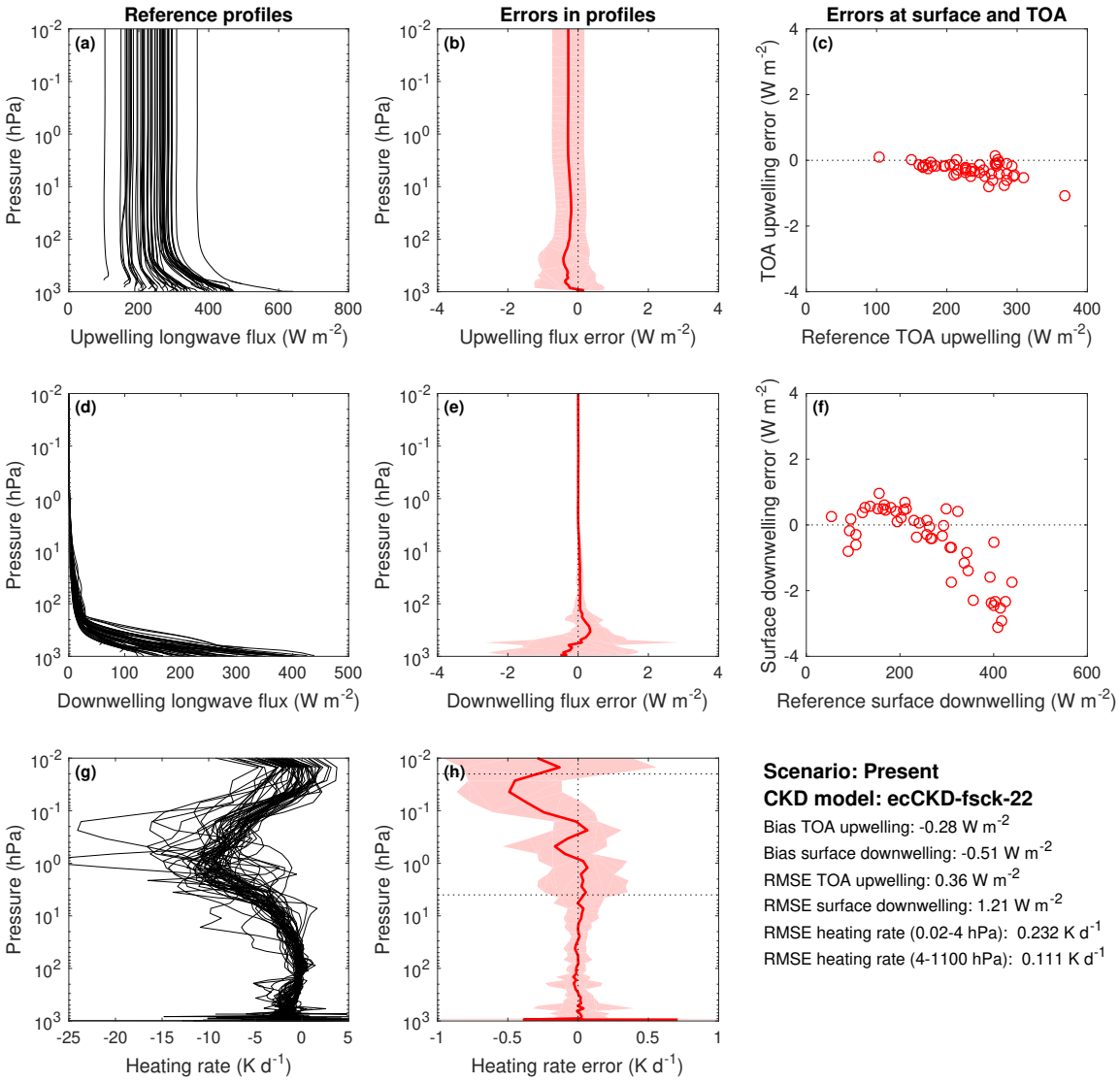

Evaluation of the global-nwp-fsck-22 CKD model for the "present-day" CKDMIP scenario. The left three panels show the irradiances and heating rates from the reference line-by-line calculations. The red lines in the middle three panels show the corresponding bias in these quantities from the CKD model. The shaded regions encompass 95% of the instantaneous errors. Panels c and f depict instantaneous errors in upwelling TOA and downwelling surface irradiances. Error metrics are provided in the lower right.

Model 4: ecCKD global-nwp-fsck-30

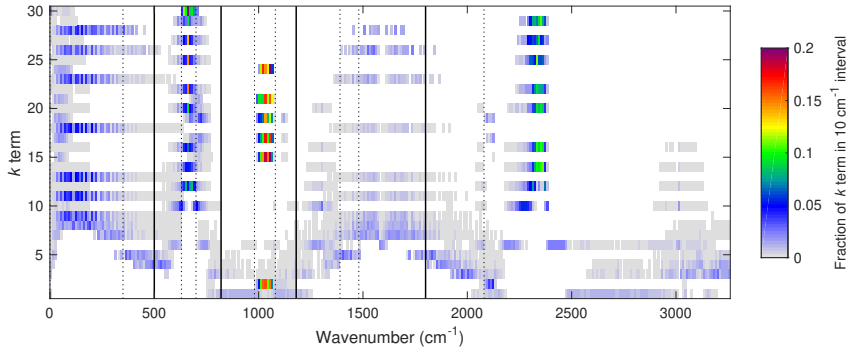

Illustration of the parts of the longwave spectrum that contribute to each k term of the global-nwp-fsck-30 model.

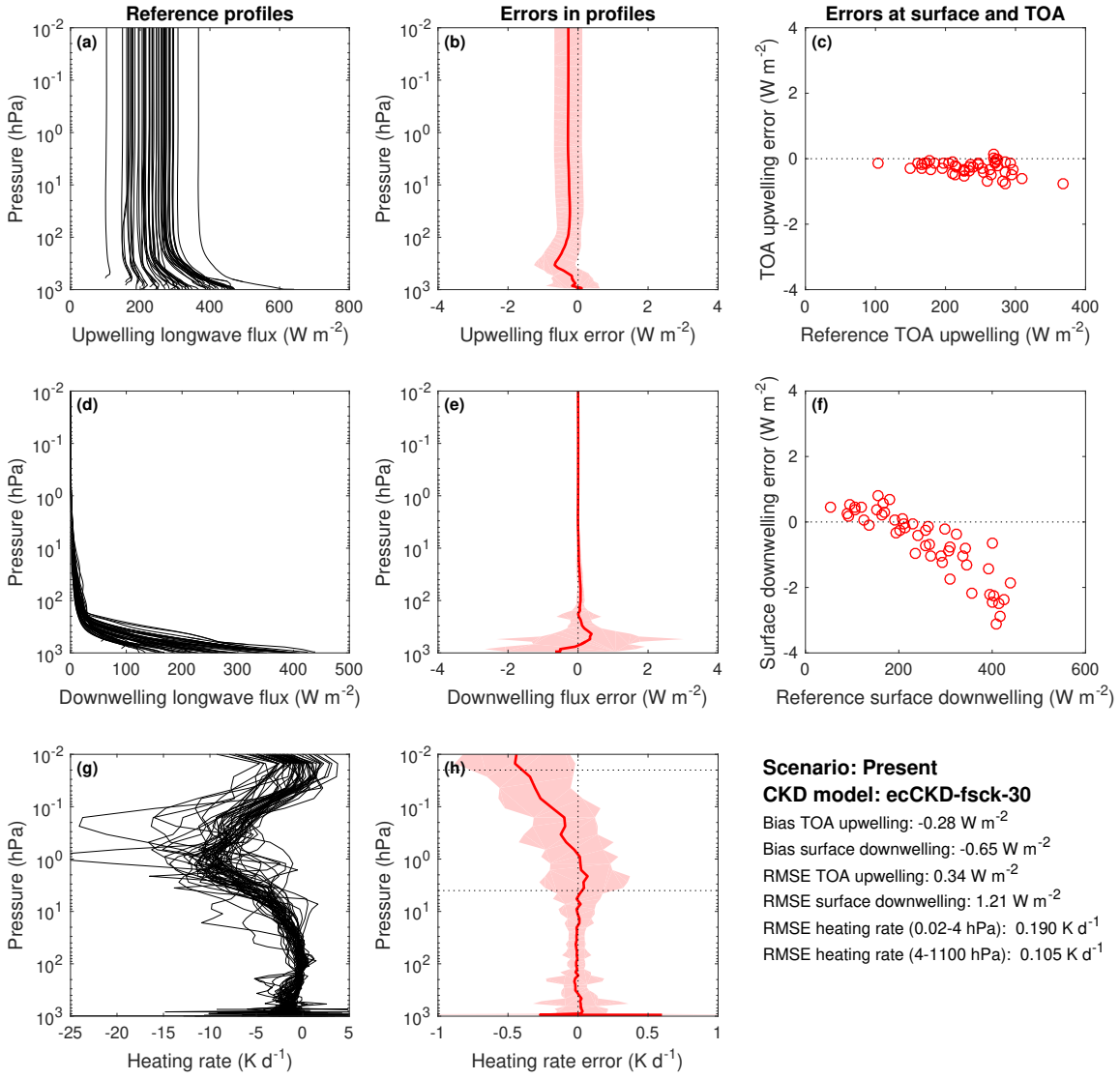

Evaluation of the global-nwp-fsck-30 CKD model for the "present-day" CKDMIP scenario. The left three panels show the irradiances and heating rates from the reference line-by-line calculations. The red lines in the middle three panels show the corresponding bias in these quantities from the CKD model. The shaded regions encompass 95% of the instantaneous errors. Panels c and f depict instantaneous errors in upwelling TOA and downwelling surface irradiances. Error metrics are provided in the lower right.

Model 5: ecCKD global-nwp-fsck-44

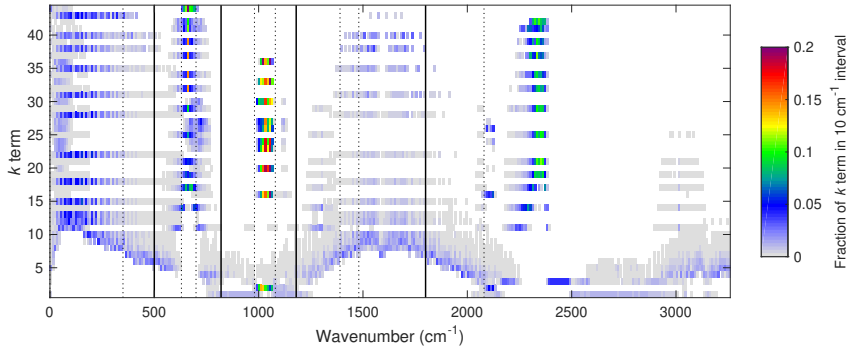

Illustration of the parts of the longwave spectrum that contribute to each k term of the global-nwp-fsck-44 model.

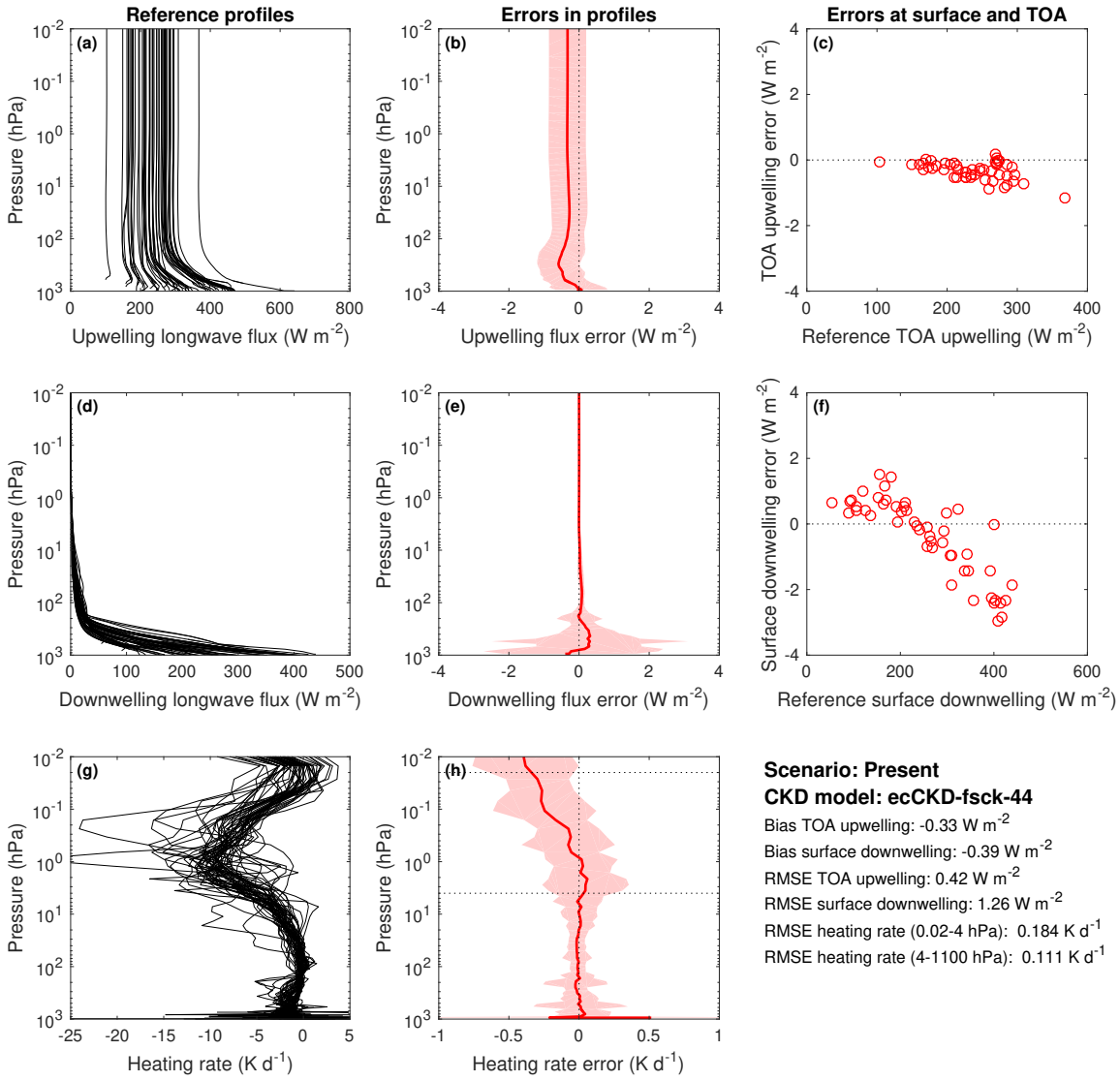

Evaluation of the global-nwp-fsck-44 CKD model for the "present-day" CKDMIP scenario. The left three panels show the irradiances and heating rates from the reference line-by-line calculations. The red lines in the middle three panels show the corresponding bias in these quantities from the CKD model. The shaded regions encompass 95% of the instantaneous errors. Panels c and f depict instantaneous errors in upwelling TOA and downwelling surface irradiances. Error metrics are provided in the lower right.

Model 6: ecCKD global-nwp-fsck-75

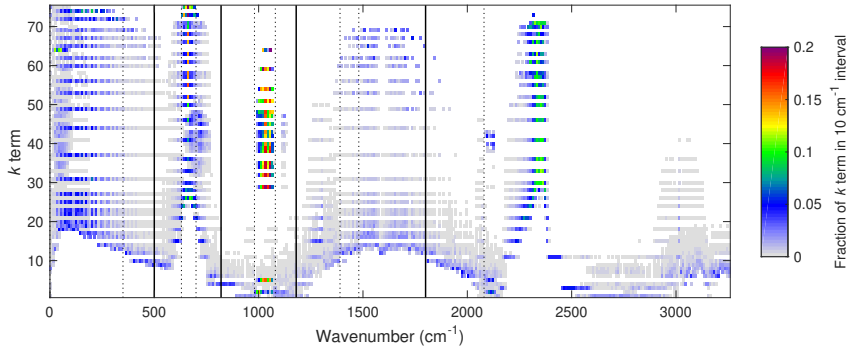

Illustration of the parts of the longwave spectrum that contribute to each k term of the global-nwp-fsck-75 model.

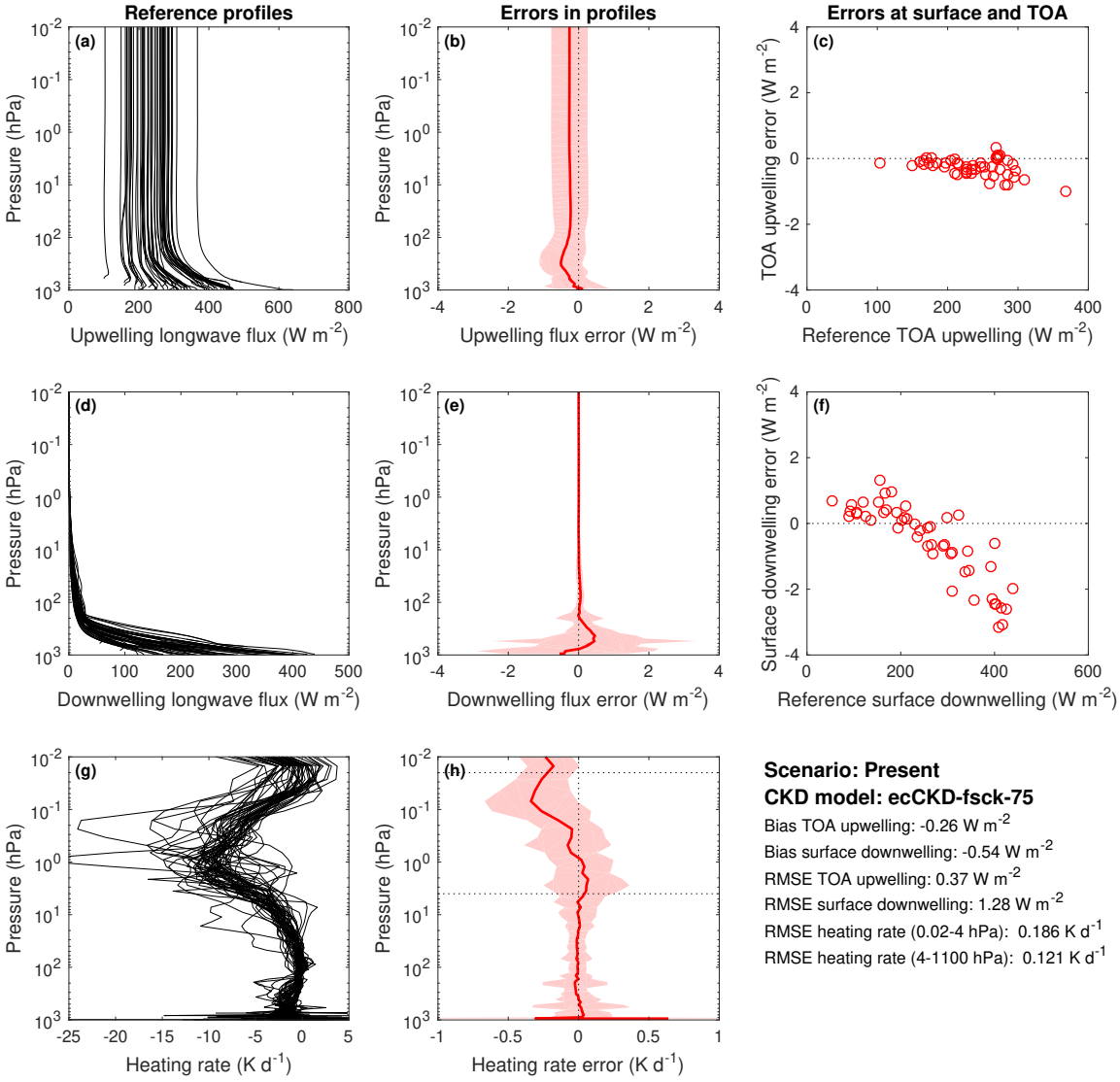

Evaluation of the global-nwp-fsck-75 CKD model for the "present-day" CKDMIP scenario. The left three panels show the irradiances and heating rates from the reference line-by-line calculations. The red lines in the middle three panels show the corresponding bias in these quantities from the CKD model. The shaded regions encompass 95% of the instantaneous errors. Panels c and f depict instantaneous errors in upwelling TOA and downwelling surface irradiances. Error metrics are provided in the lower right.

Model 7: ecCKD global-nwp-wide-11

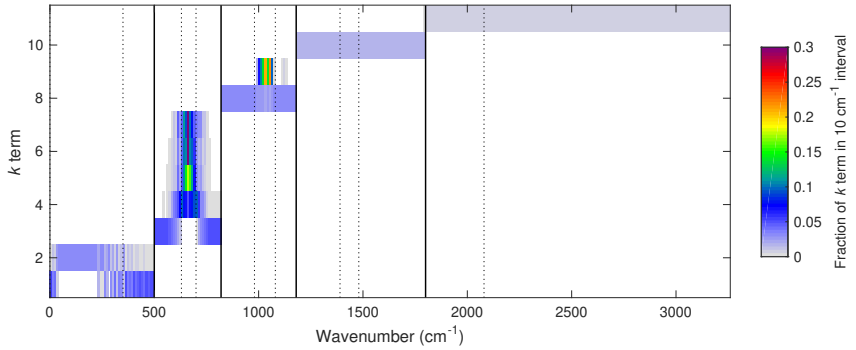

Illustration of the parts of the longwave spectrum that contribute to each k term of the global-nwp-wide-11 model.

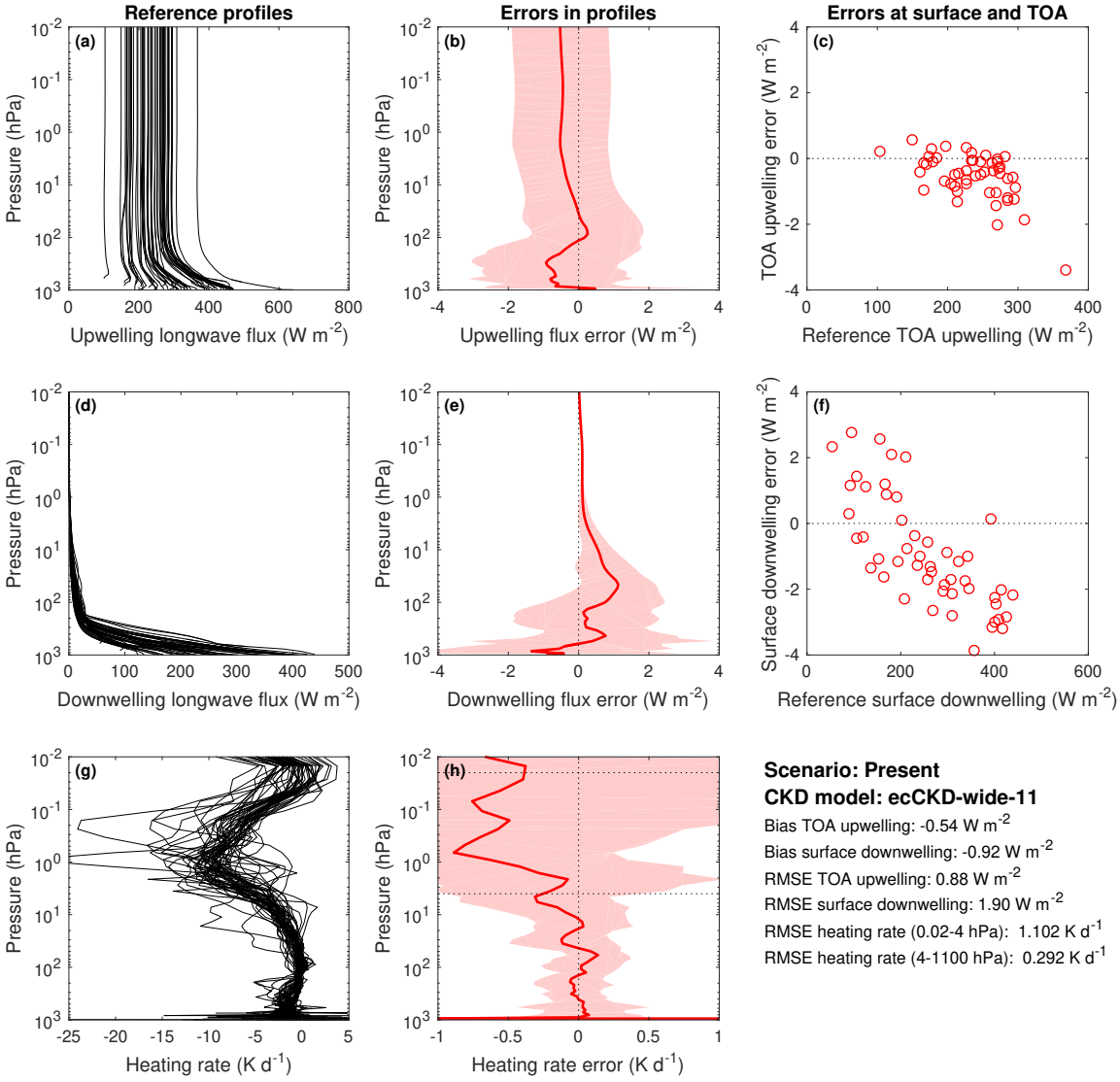

Evaluation of the global-nwp-wide-11 CKD model for the "present-day" CKDMIP scenario. The left three panels show the irradiances and heating rates from the reference line-by-line calculations. The red lines in the middle three panels show the corresponding bias in these quantities from the CKD model. The shaded regions encompass 95% of the instantaneous errors. Panels c and f depict instantaneous errors in upwelling TOA and downwelling surface irradiances. Error metrics are provided in the lower right.

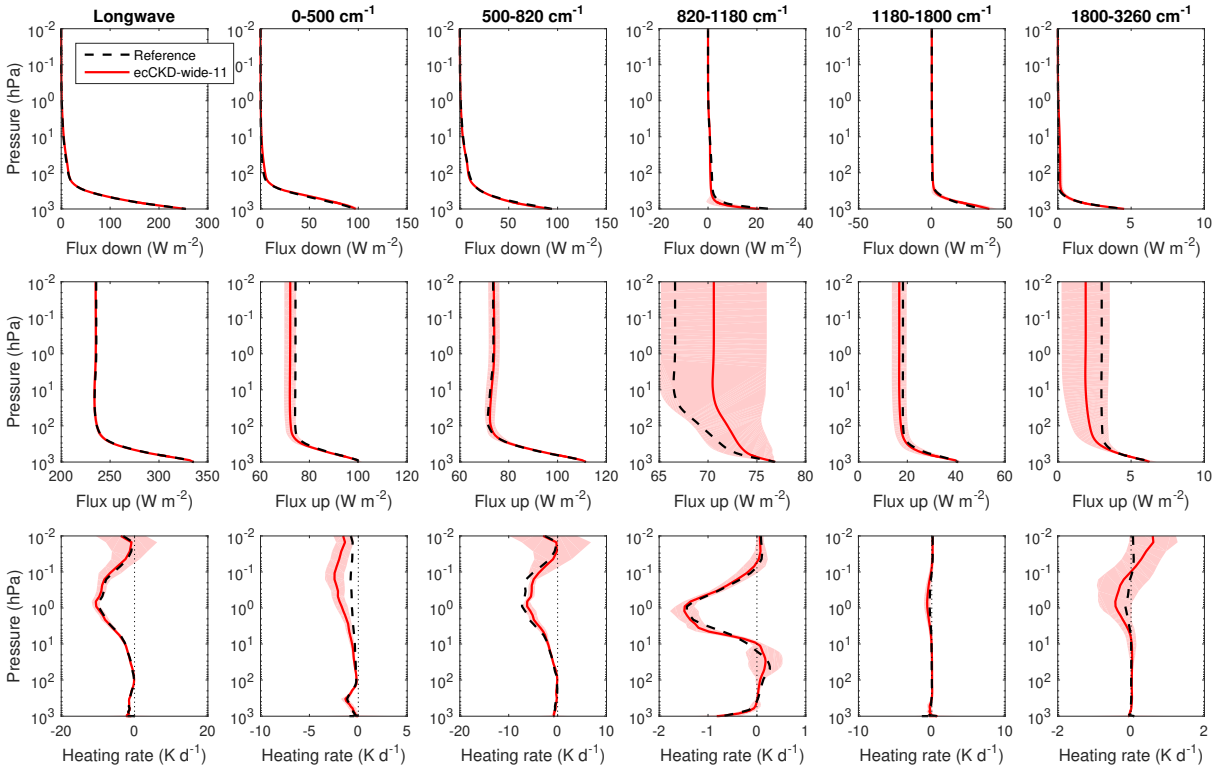

Evaluation of irradiances and heating rates for the broadband (leftmost column of panels) and the 5 wide longwave bands (other panels) of the global-nwp-wide-11 CKD model. The black dashed and red solid lines correspond to the average of the 50 profiles for the "present-day" scenario, while the shaded regions encompass 95% of the error.

Model 8: ecCKD global-nwp-wide-16

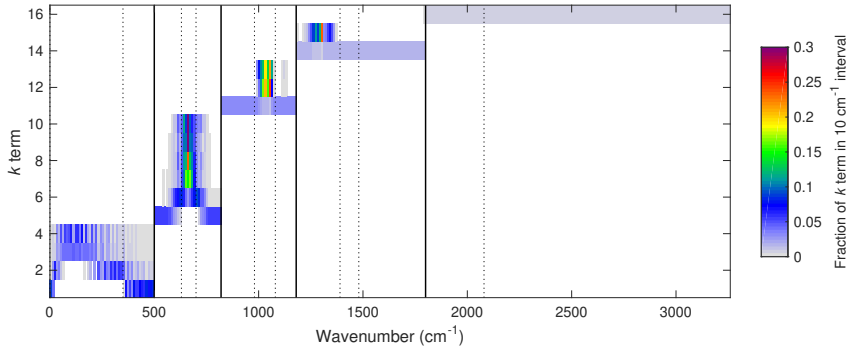

Illustration of the parts of the longwave spectrum that contribute to each k term of the global-nwp-wide-16 model.

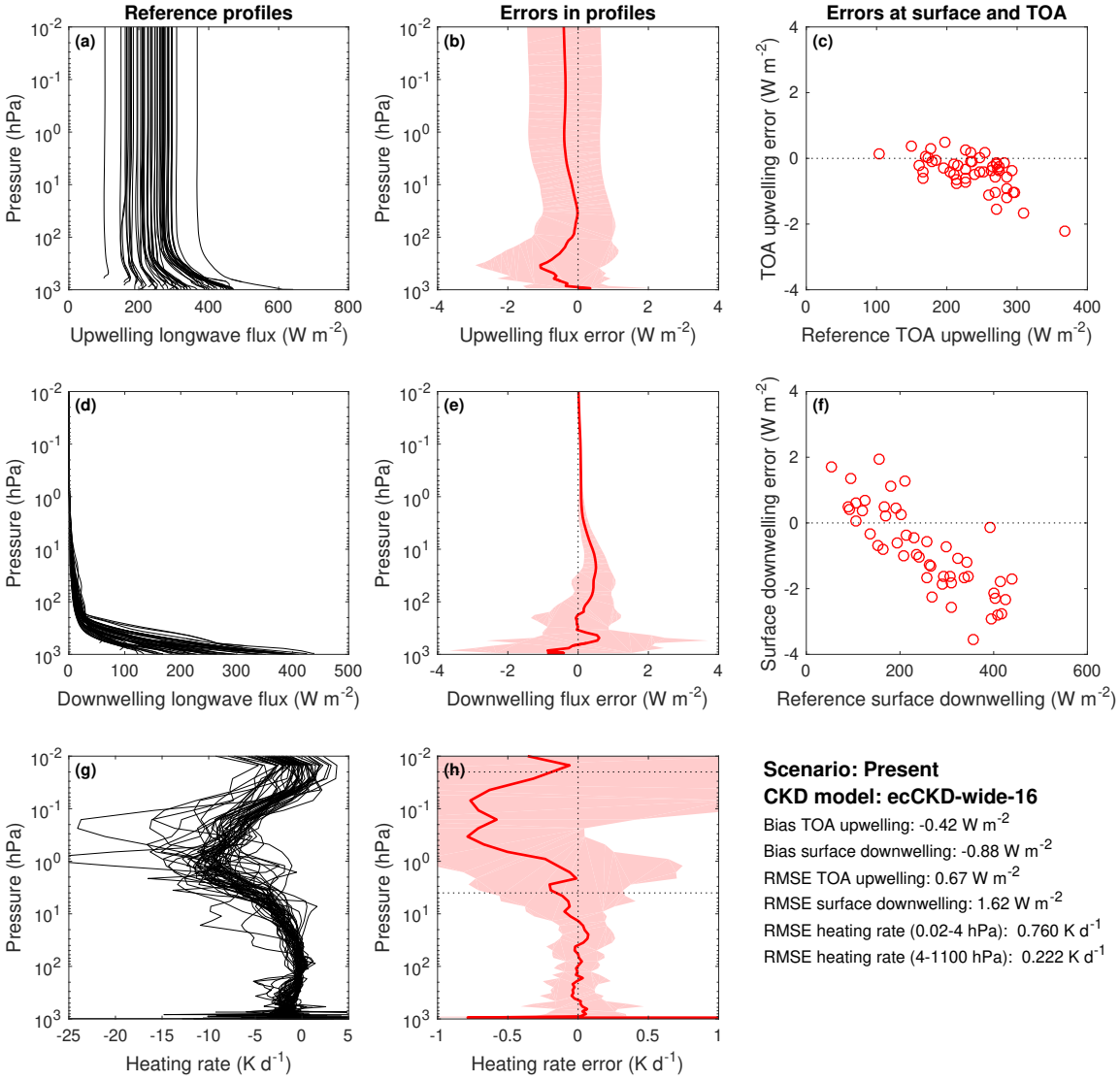

Evaluation of the global-nwp-wide-16 CKD model for the "present-day" CKDMIP scenario. The left three panels show the irradiances and heating rates from the reference line-by-line calculations. The red lines in the middle three panels show the corresponding bias in these quantities from the CKD model. The shaded regions encompass 95% of the instantaneous errors. Panels c and f depict instantaneous errors in upwelling TOA and downwelling surface irradiances. Error metrics are provided in the lower right.

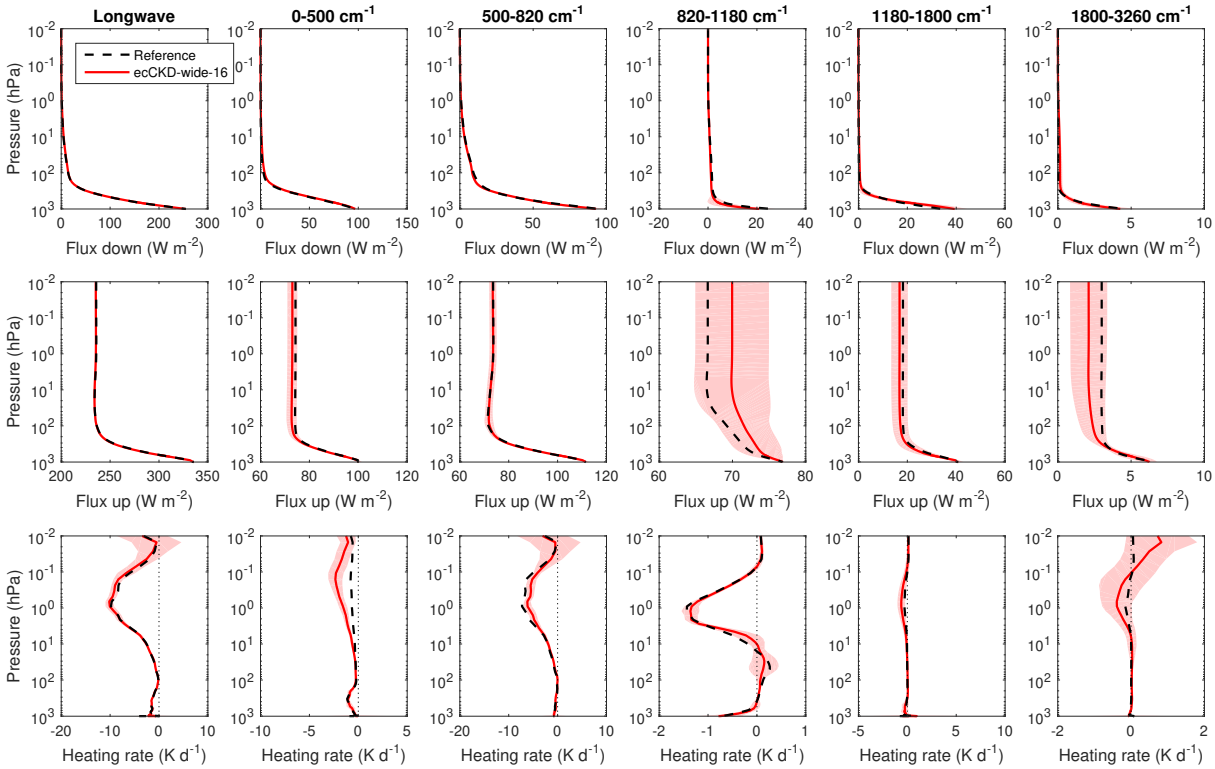

Evaluation of irradiances and heating rates for the broadband (leftmost column of panels) and the 5 wide longwave bands (other panels) of the global-nwp-wide-16 CKD model. The black dashed and red solid lines correspond to the average of the 50 profiles for the "present-day" scenario, while the shaded regions encompass 95% of the error.

Model 9: ecCKD global-nwp-wide-28

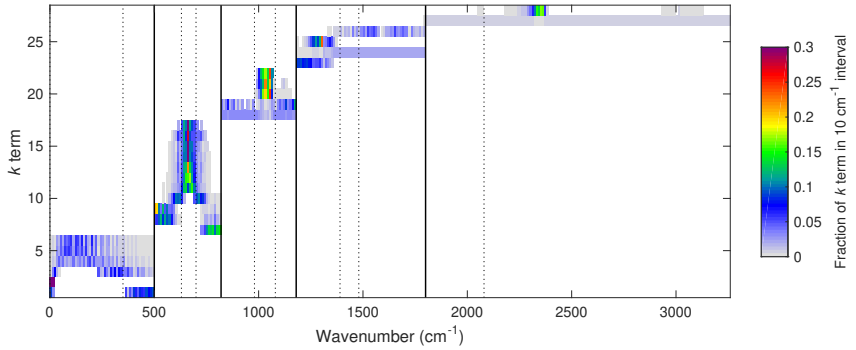

Illustration of the parts of the longwave spectrum that contribute to each k term of the global-nwp-wide-28 model.

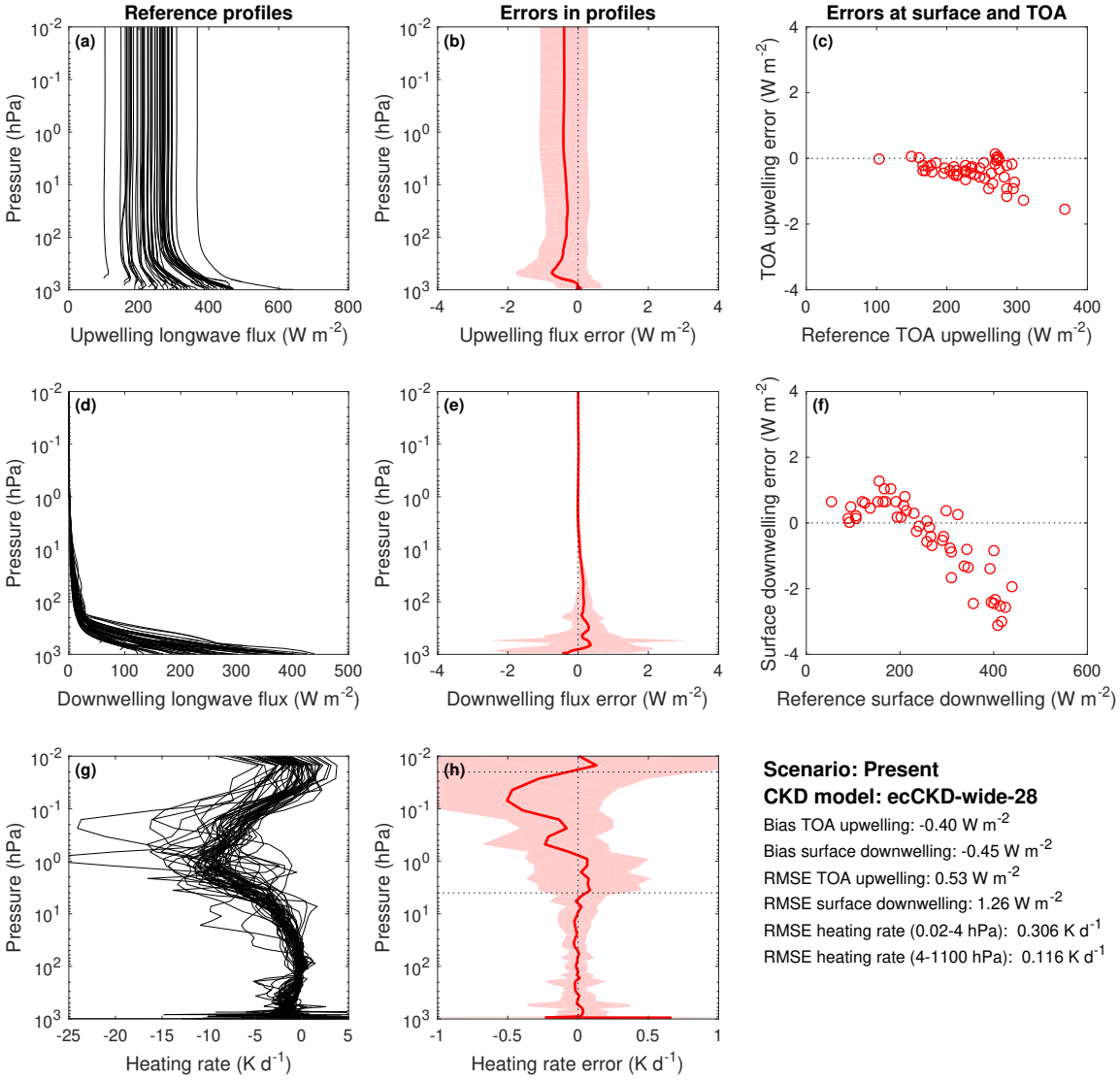

Evaluation of the global-nwp-wide-28 CKD model for the "present-day" CKDMIP scenario. The left three panels show the irradiances and heating rates from the reference line-by-line calculations. The red lines in the middle three panels show the corresponding bias in these quantities from the CKD model. The shaded regions encompass 95% of the instantaneous errors. Panels c and f depict instantaneous errors in upwelling TOA and downwelling surface irradiances. Error metrics are provided in the lower right.

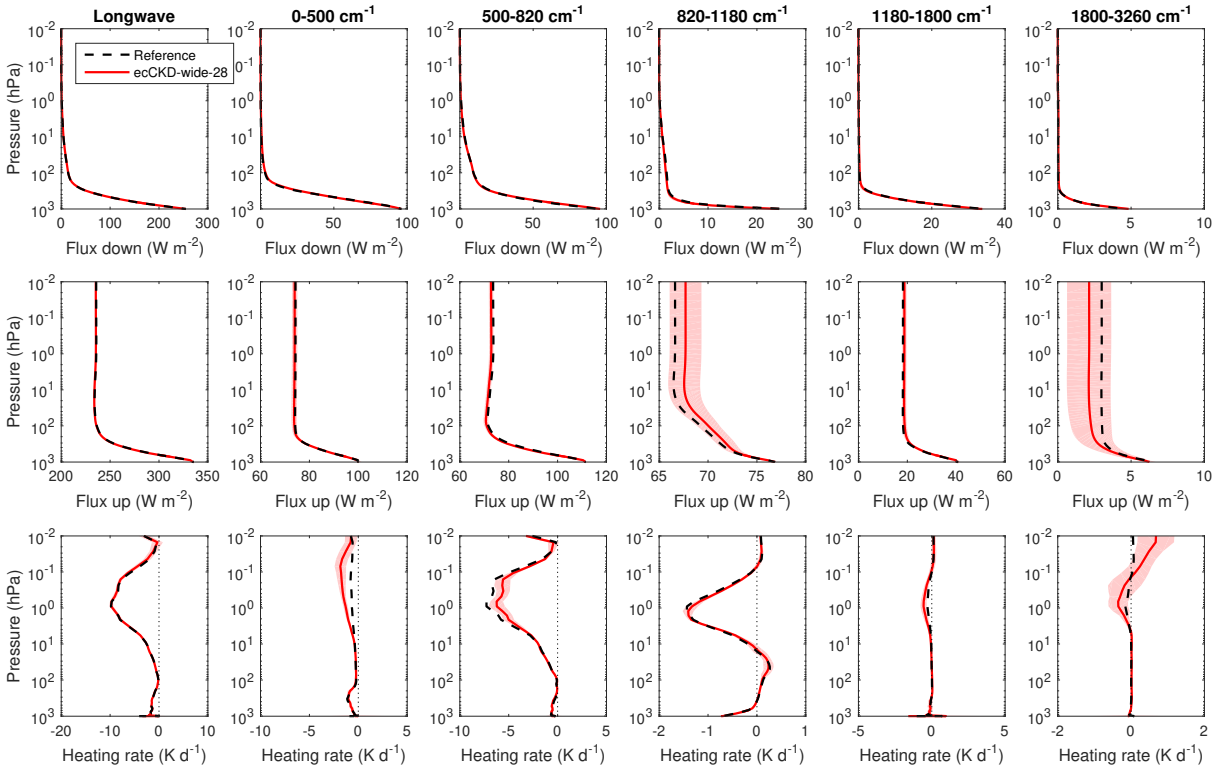

Evaluation of irradiances and heating rates for the broadband (leftmost column of panels) and the 5 wide longwave bands (other panels) of the global-nwp-wide-28 CKD model. The black dashed and red solid lines correspond to the average of the 50 profiles for the "present-day" scenario, while the shaded regions encompass 95% of the error.

Model 10: ecCKD global-nwp-wide-38

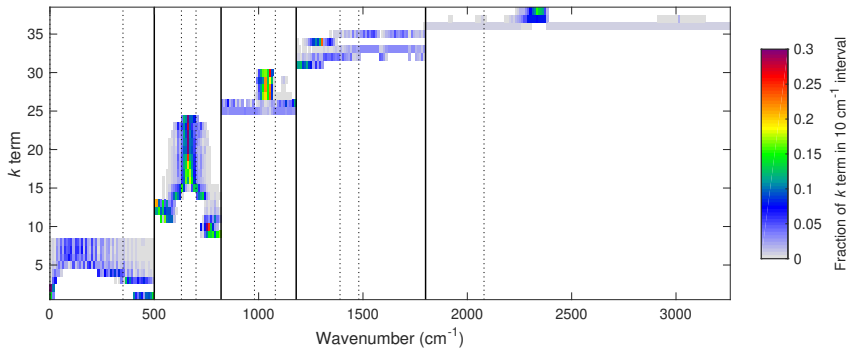

Illustration of the parts of the longwave spectrum that contribute to each k term of the global-nwp-wide-38 model.

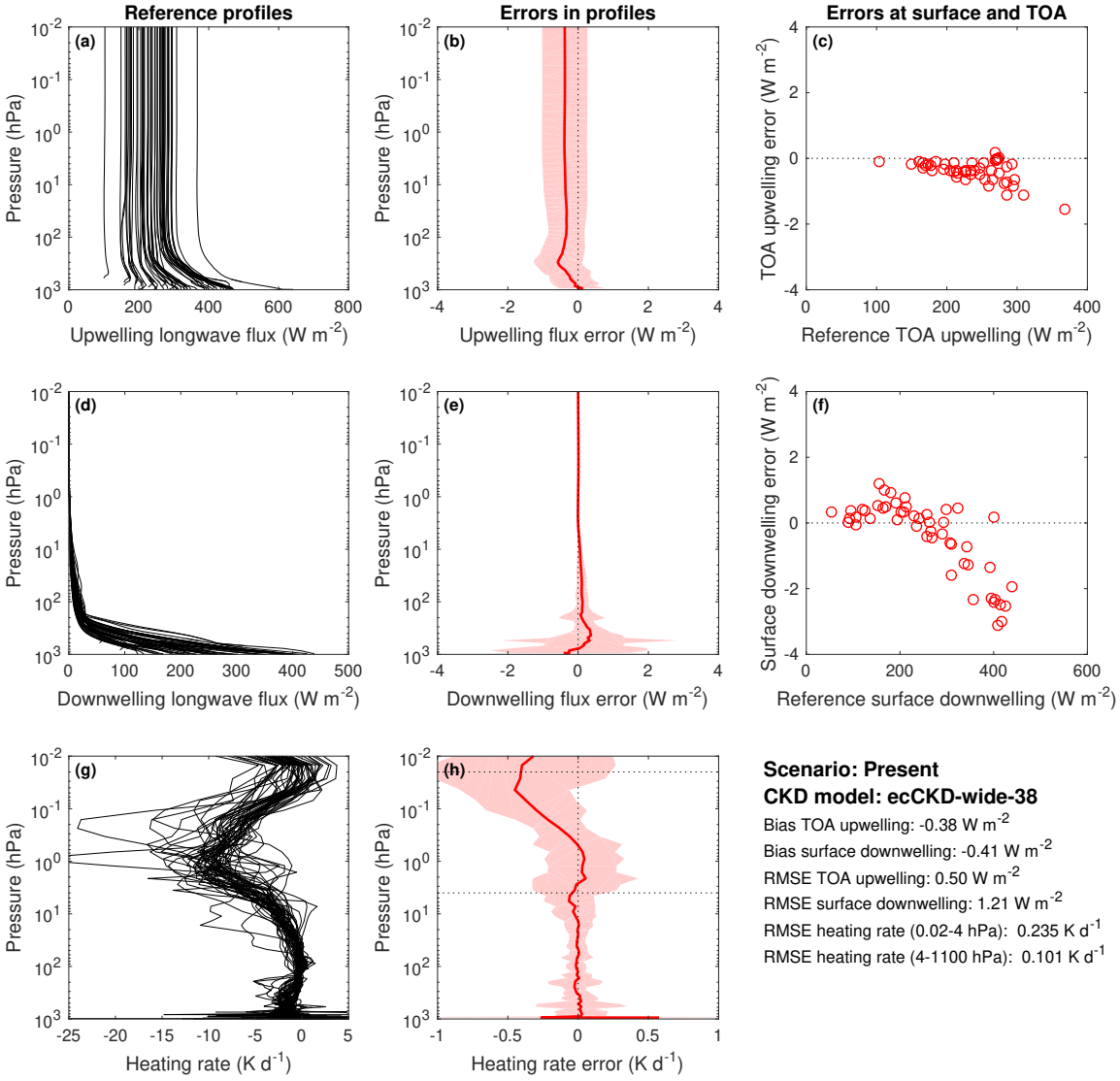

Evaluation of the global-nwp-wide-38 CKD model for the "present-day" CKDMIP scenario. The left three panels show the irradiances and heating rates from the reference line-by-line calculations. The red lines in the middle three panels show the corresponding bias in these quantities from the CKD model. The shaded regions encompass 95% of the instantaneous errors. Panels c and f depict instantaneous errors in upwelling TOA and downwelling surface irradiances. Error metrics are provided in the lower right.

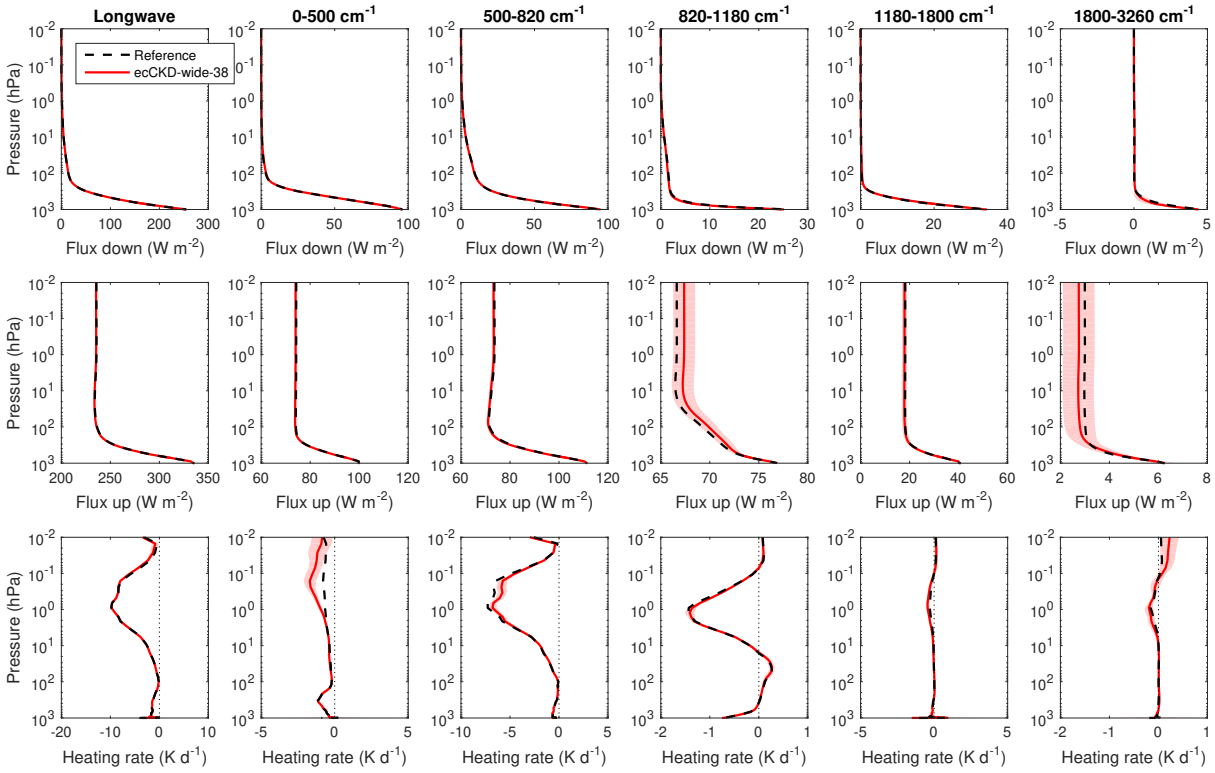

Evaluation of irradiances and heating rates for the broadband (leftmost column of panels) and the 5 wide longwave bands (other panels) of the global-nwp-wide-38 CKD model. The black dashed and red solid lines correspond to the average of the 50 profiles for the "present-day" scenario, while the shaded regions encompass 95% of the error.

Model 11: ecCKD global-nwp-wide-49

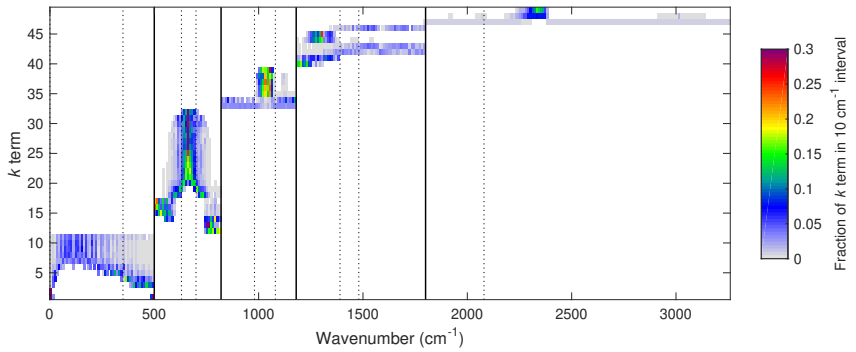

Illustration of the parts of the longwave spectrum that contribute to each k term of the global-nwp-wide-49 model.

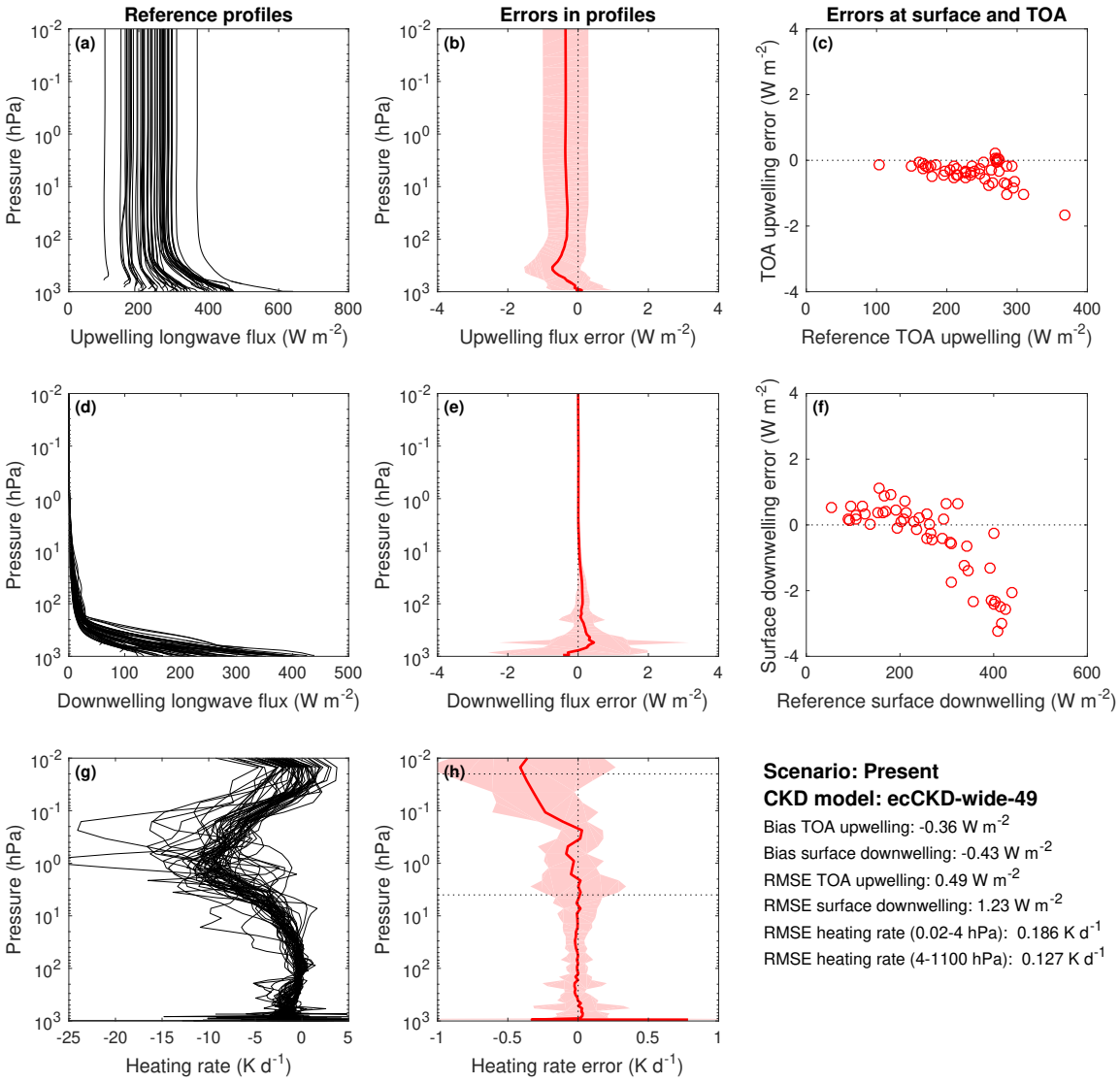

Evaluation of the global-nwp-wide-49 CKD model for the "present-day" CKDMIP scenario. The left three panels show the irradiances and heating rates from the reference line-by-line calculations. The red lines in the middle three panels show the corresponding bias in these quantities from the CKD model. The shaded regions encompass 95% of the instantaneous errors. Panels c and f depict instantaneous errors in upwelling TOA and downwelling surface irradiances. Error metrics are provided in the lower right.

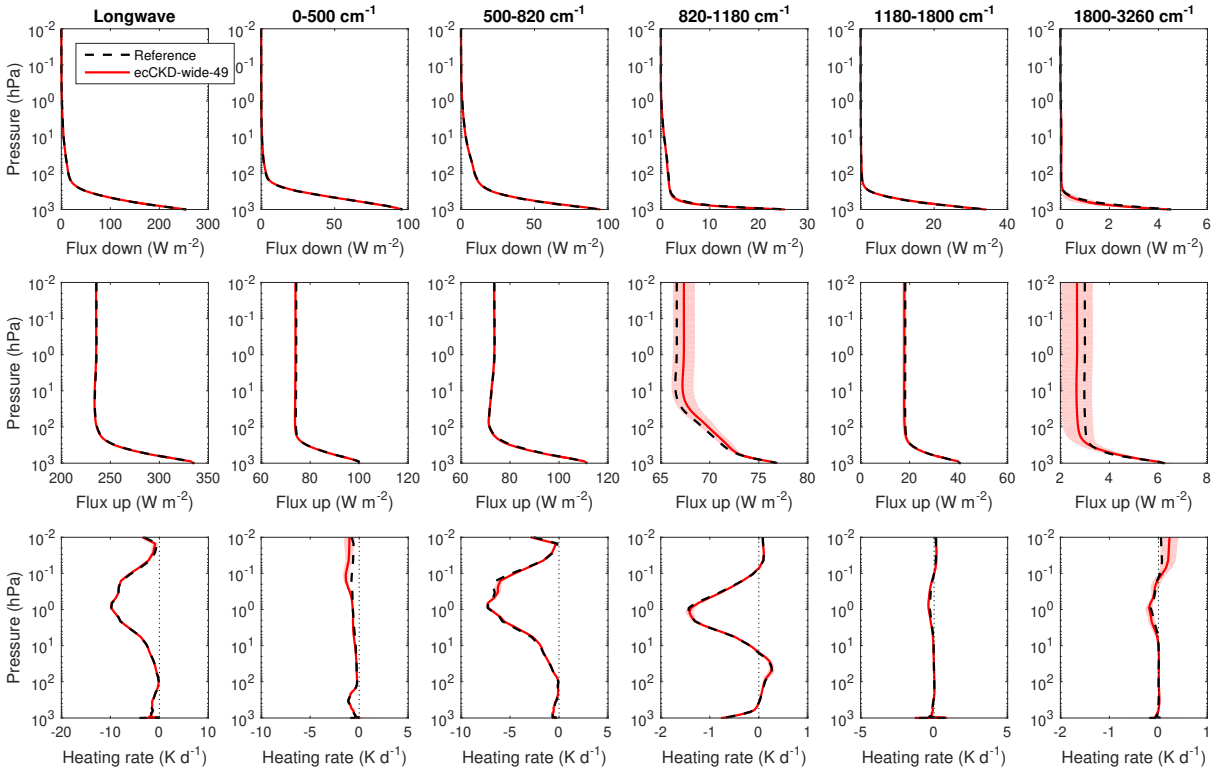

Evaluation of irradiances and heating rates for the broadband (leftmost column of panels) and the 5 wide longwave bands (other panels) of the global-nwp-wide-49 CKD model. The black dashed and red solid lines correspond to the average of the 50 profiles for the "present-day" scenario, while the shaded regions encompass 95% of the error.

Model 12: ecCKD global-nwp-wide-74

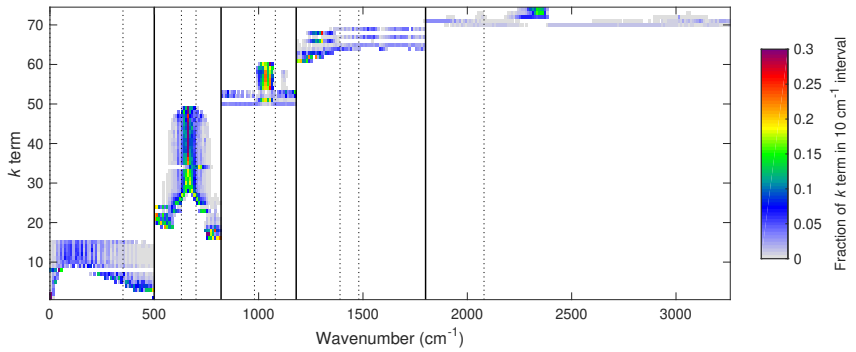

Illustration of the parts of the longwave spectrum that contribute to each k term of the global-nwp-wide-74 model.

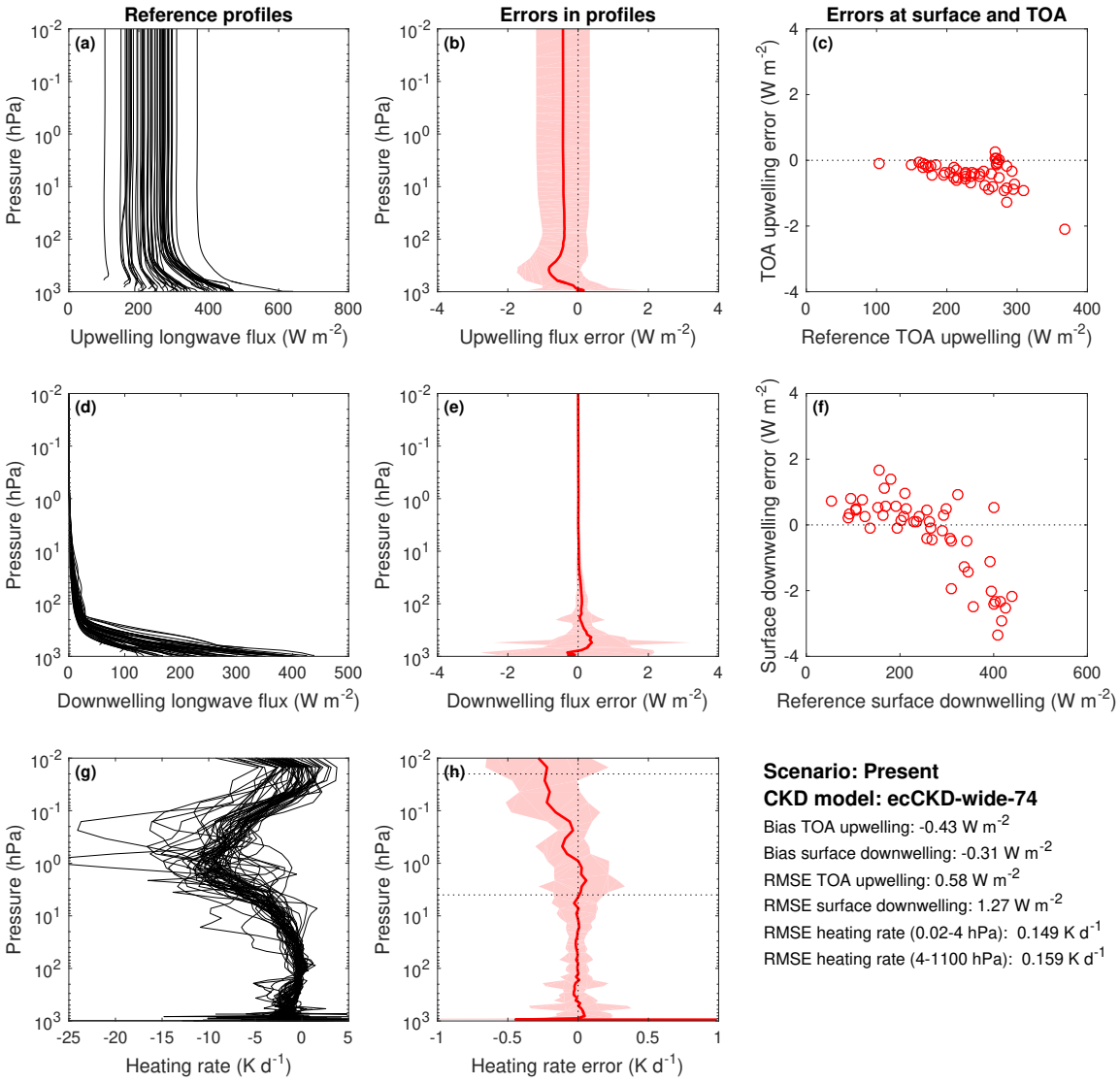

Evaluation of the global-nwp-wide-74 CKD model for the "present-day" CKDMIP scenario. The left three panels show the irradiances and heating rates from the reference line-by-line calculations. The red lines in the middle three panels show the corresponding bias in these quantities from the CKD model. The shaded regions encompass 95% of the instantaneous errors. Panels c and f depict instantaneous errors in upwelling TOA and downwelling surface irradiances. Error metrics are provided in the lower right.

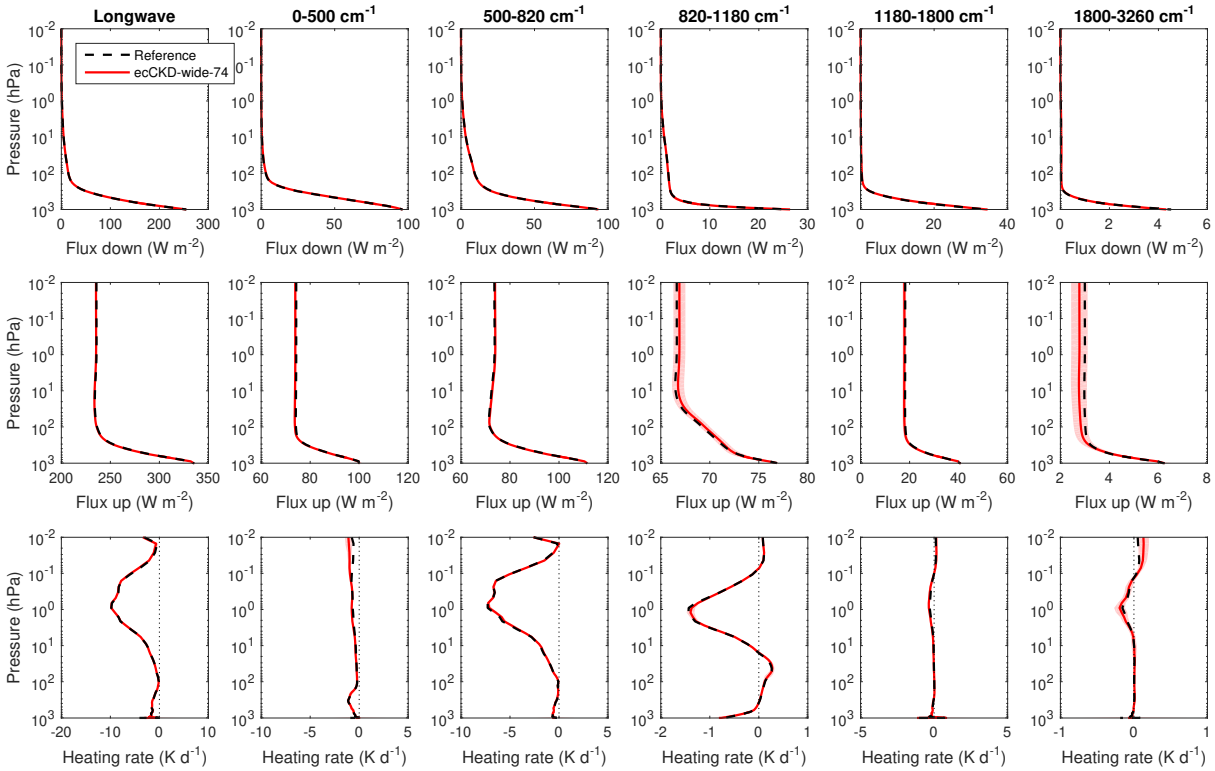

Evaluation of irradiances and heating rates for the broadband (leftmost column of panels) and the 5 wide longwave bands (other panels) of the global-nwp-wide-74 CKD model. The black dashed and red solid lines correspond to the average of the 50 profiles for the "present-day" scenario, while the shaded regions encompass 95% of the error.

Model 13: ecCKD global-nwp-narrow-20

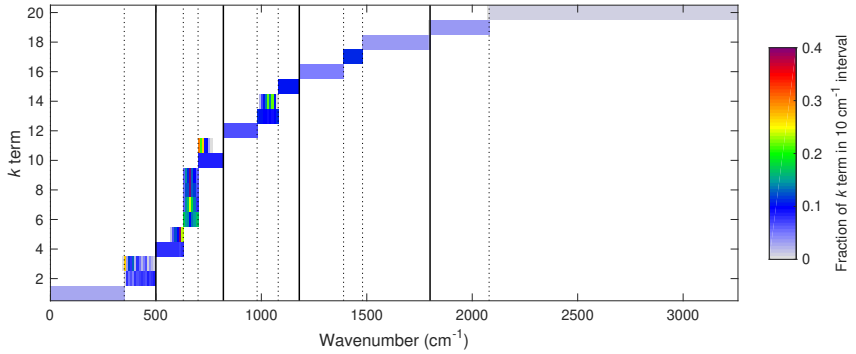

Illustration of the parts of the longwave spectrum that contribute to each k term of the global-nwp-narrow-20 model.

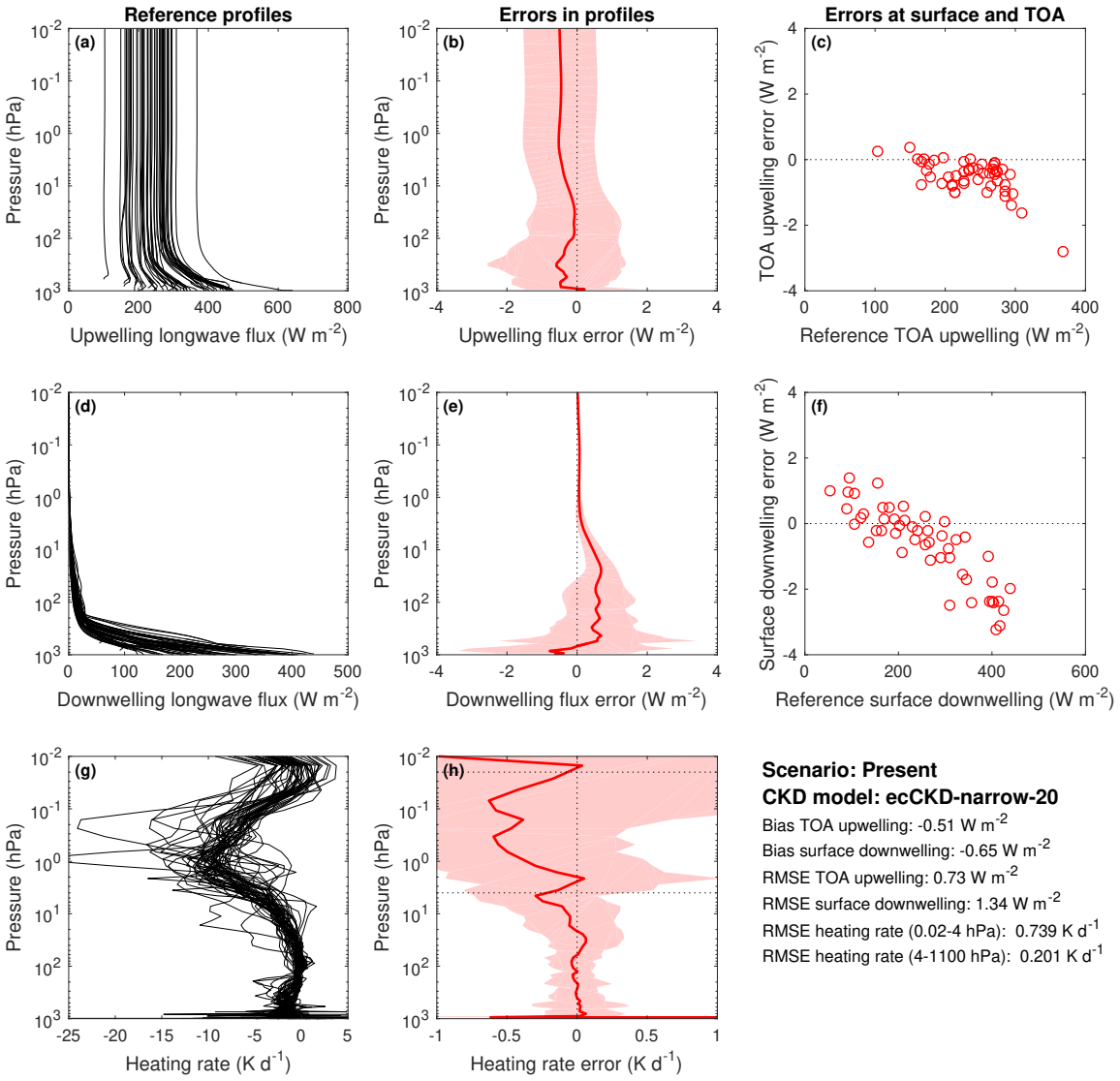

Evaluation of the global-nwp-narrow-20 CKD model for the "present-day" CKDMIP scenario. The left three panels show the irradiances and heating rates from the reference line-by-line calculations. The red lines in the middle three panels show the corresponding bias in these quantities from the CKD model. The shaded regions encompass 95% of the instantaneous errors. Panels c and f depict instantaneous errors in upwelling TOA and downwelling surface irradiances. Error metrics are provided in the lower right.

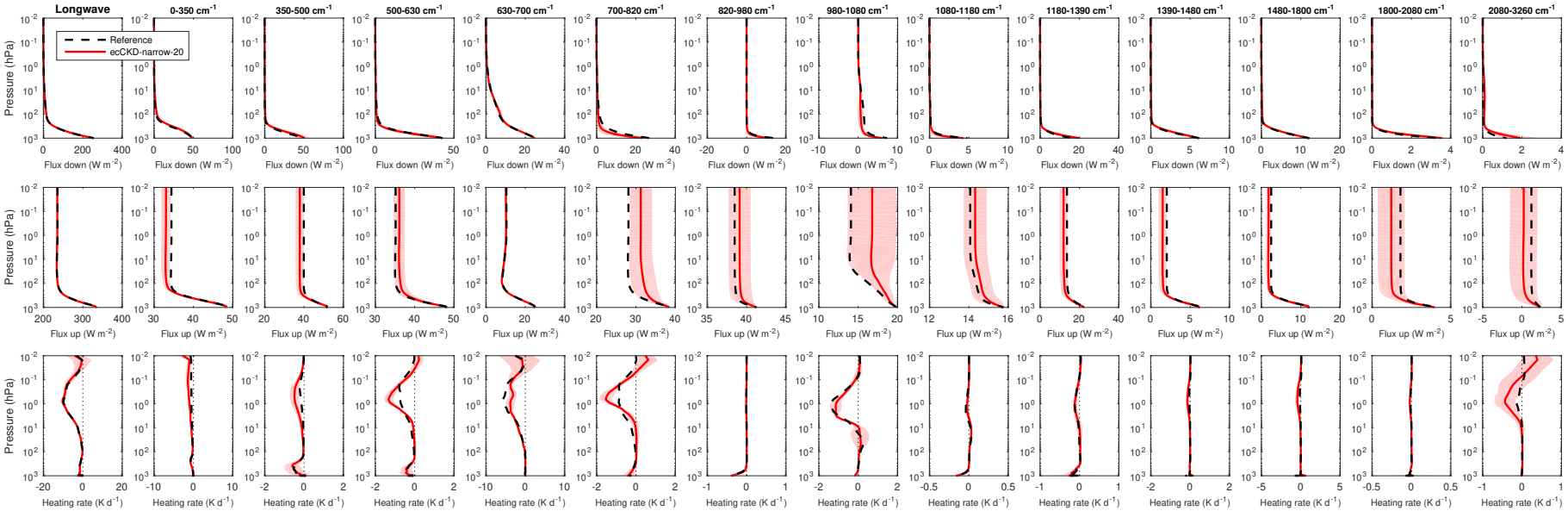

Evaluation of irradiances and heating rates for the broadband (leftmost column of panels) and the 13 narrow longwave bands (other panels) of the global-nwp-narrow-20 CKD model. The black dashed and red solid lines correspond to the average of the 50 profiles for the "present-day" scenario, while the shaded regions encompass 95% of the error.

Model 14: ecCKD global-nwp-narrow-27

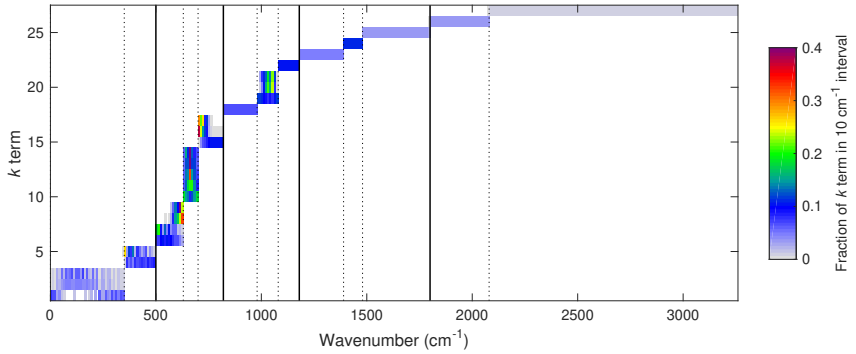

Illustration of the parts of the longwave spectrum that contribute to each k term of the global-nwp-narrow-27 model.

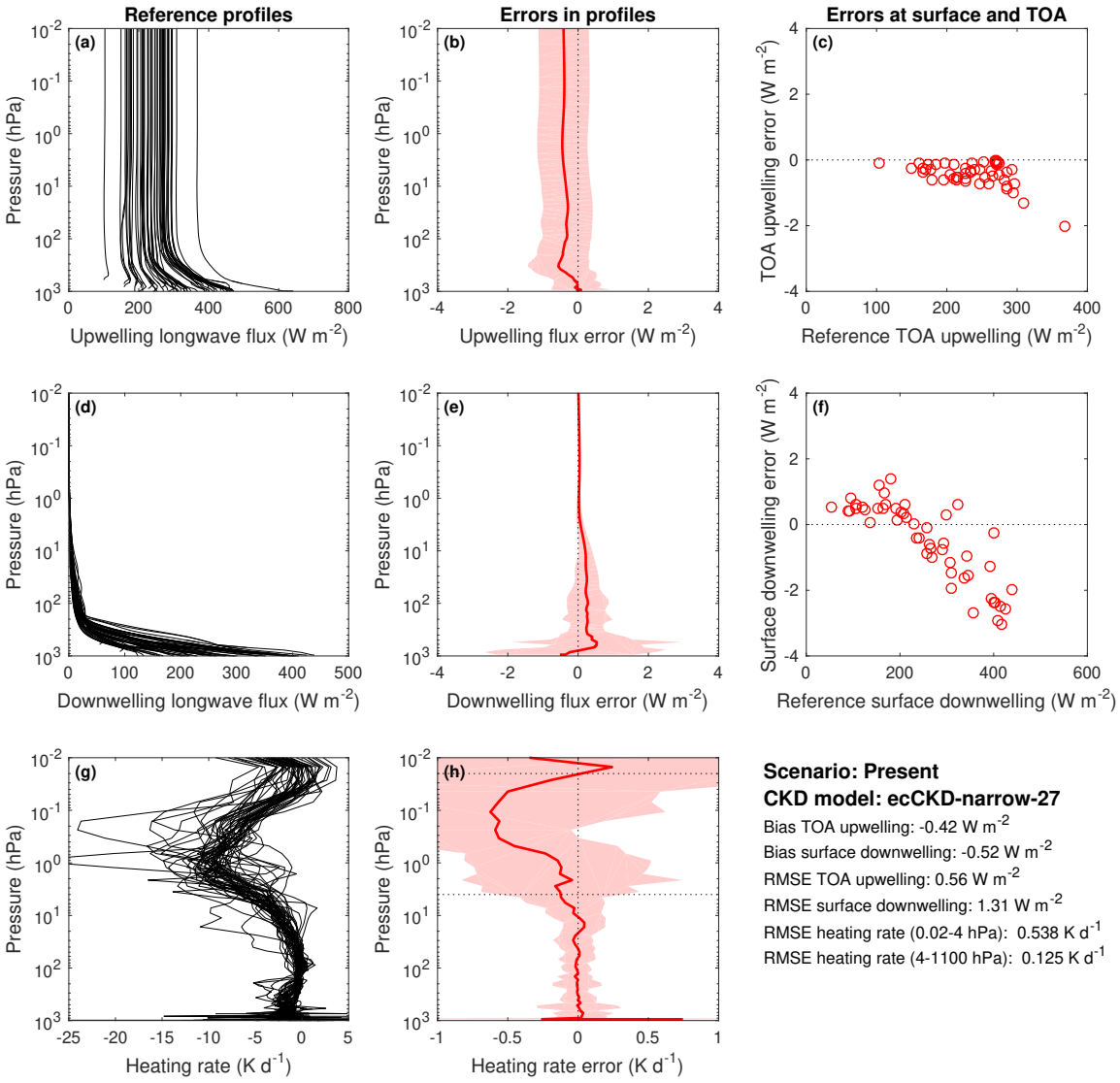

Evaluation of the global-nwp-narrow-27 CKD model for the "present-day" CKDMIP scenario. The left three panels show the irradiances and heating rates from the reference line-by-line calculations. The red lines in the middle three panels show the corresponding bias in these quantities from the CKD model. The shaded regions encompass 95% of the instantaneous errors. Panels c and f depict instantaneous errors in upwelling TOA and downwelling surface irradiances. Error metrics are provided in the lower right.

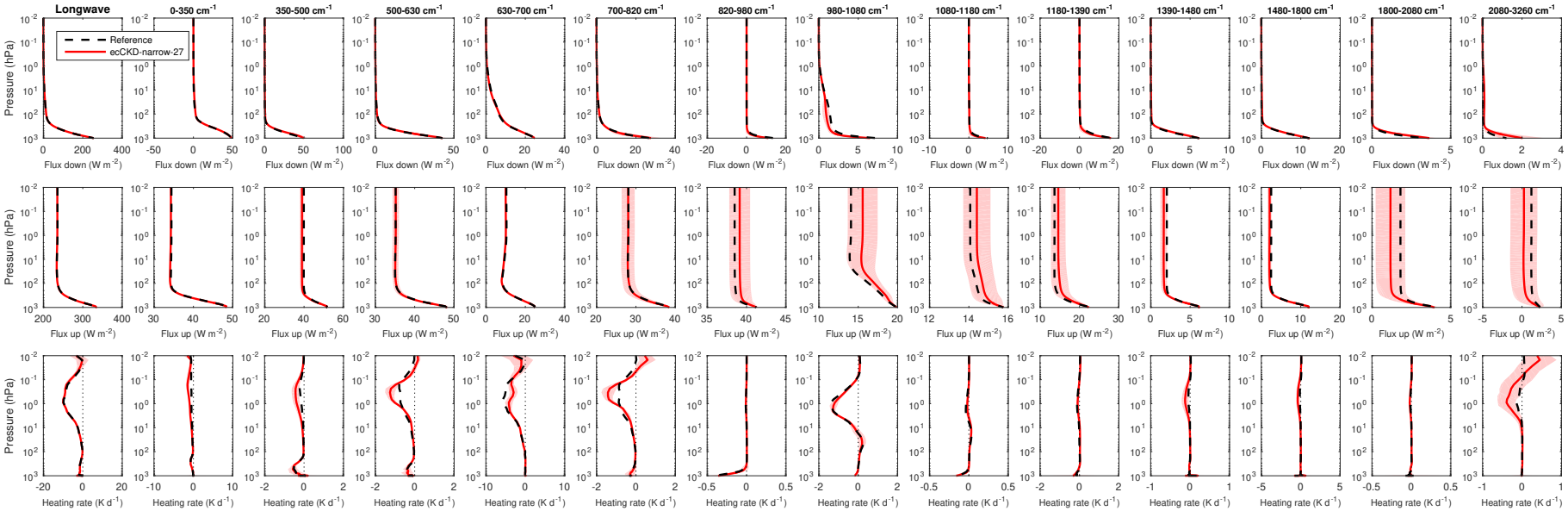

Evaluation of irradiances and heating rates for the broadband (leftmost column of panels) and the 13 narrow longwave bands (other panels) of the global-nwp-narrow-27 CKD model. The black dashed and red solid lines correspond to the average of the 50 profiles for the "present-day" scenario, while the shaded regions encompass 95% of the error.

Model 15: ecCKD global-nwp-narrow-36

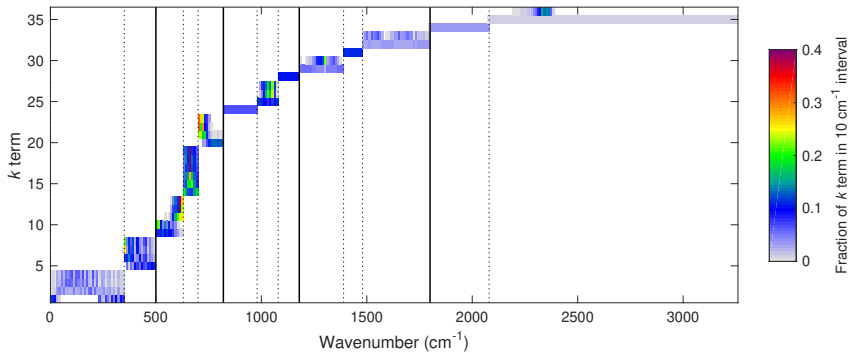

Illustration of the parts of the longwave spectrum that contribute to each k term of the global-nwp-narrow-36 model.

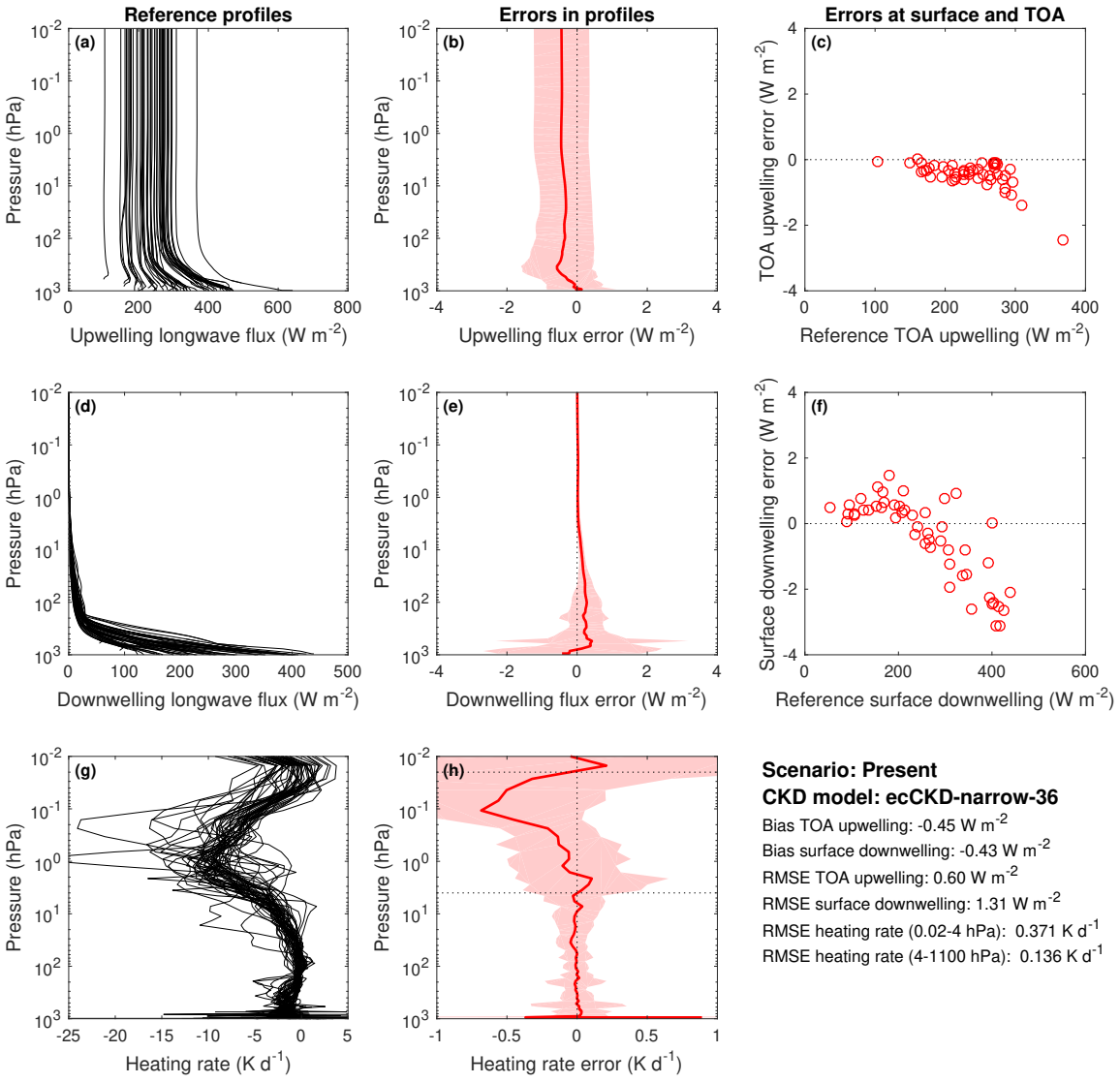

Evaluation of the global-nwp-narrow-36 CKD model for the "present-day" CKDMIP scenario. The left three panels show the irradiances and heating rates from the reference line-by-line calculations. The red lines in the middle three panels show the corresponding bias in these quantities from the CKD model. The shaded regions encompass 95% of the instantaneous errors. Panels c and f depict instantaneous errors in upwelling TOA and downwelling surface irradiances. Error metrics are provided in the lower right.

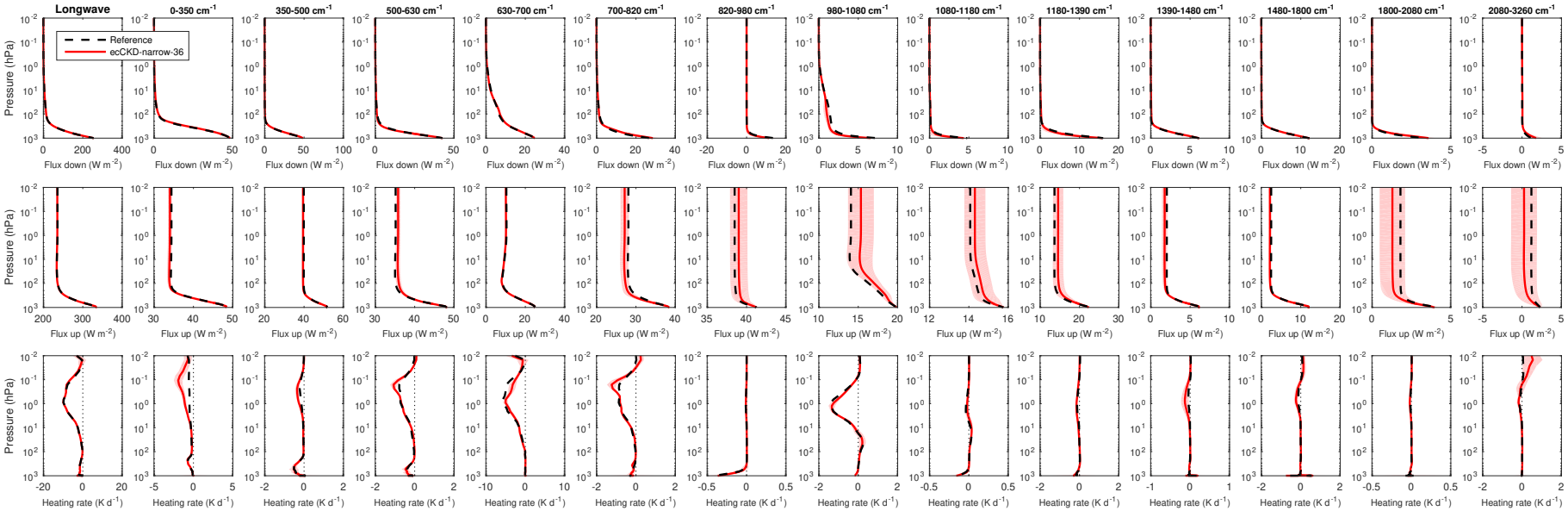

Evaluation of irradiances and heating rates for the broadband (leftmost column of panels) and the 13 narrow longwave bands (other panels) of the global-nwp-narrow-36 CKD model. The black dashed and red solid lines correspond to the average of the 50 profiles for the "present-day" scenario, while the shaded regions encompass 95% of the error.

Model 16: ecCKD global-nwp-narrow-48

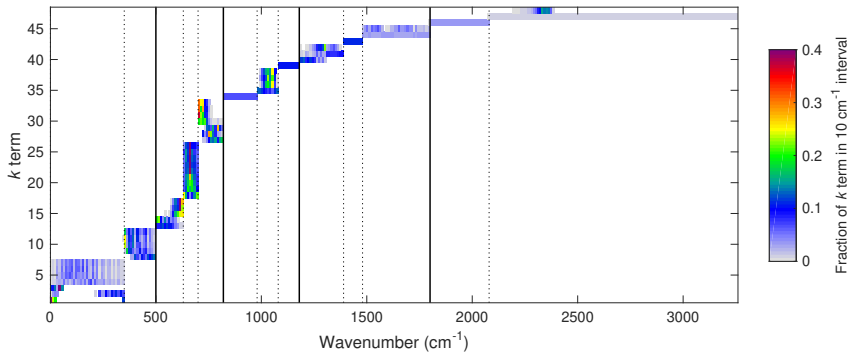

Illustration of the parts of the longwave spectrum that contribute to each k term of the global-nwp-narrow-48 model.

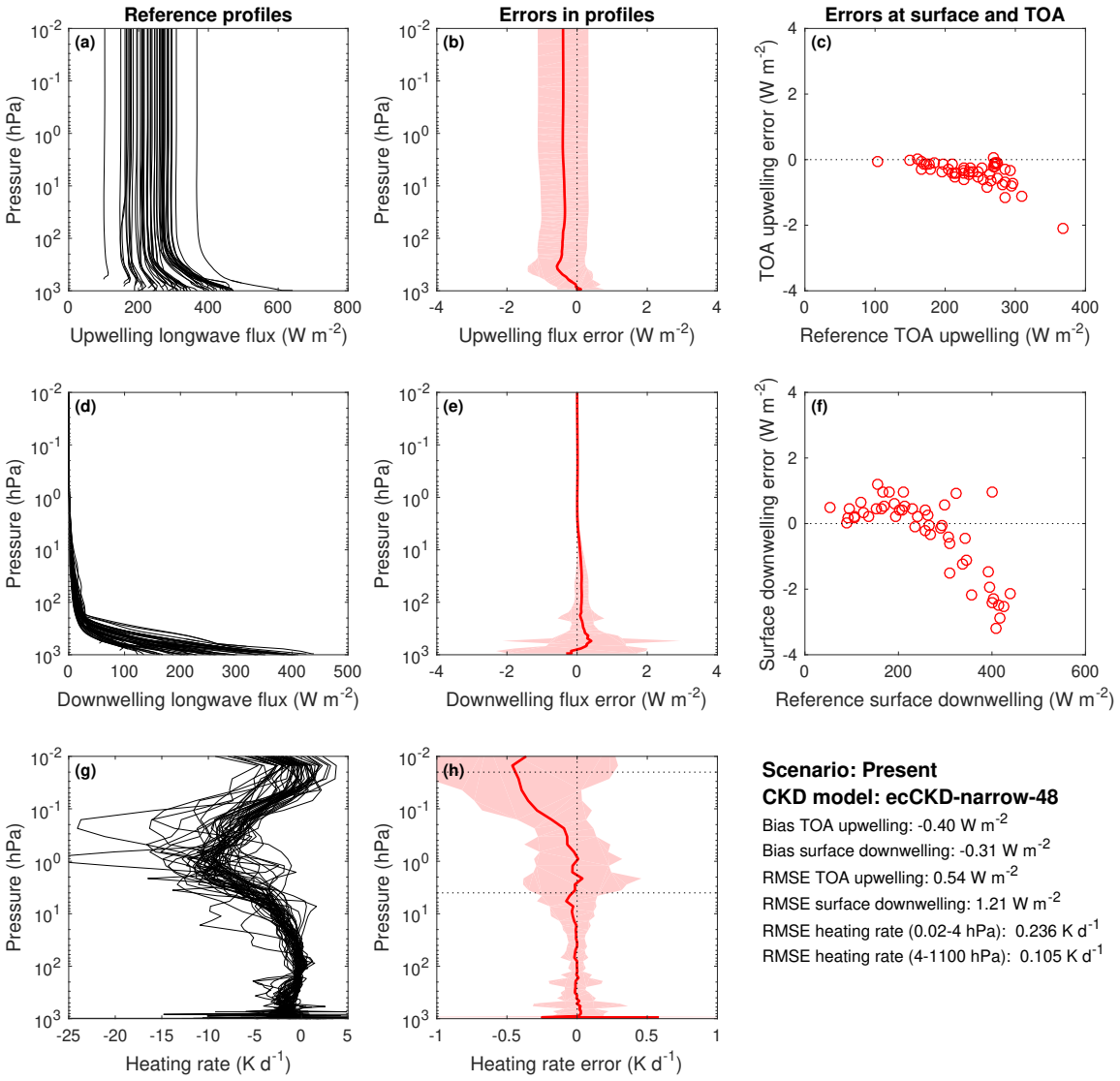

Evaluation of the global-nwp-narrow-48 CKD model for the "present-day" CKDMIP scenario. The left three panels show the irradiances and heating rates from the reference line-by-line calculations. The red lines in the middle three panels show the corresponding bias in these quantities from the CKD model. The shaded regions encompass 95% of the instantaneous errors. Panels c and f depict instantaneous errors in upwelling TOA and downwelling surface irradiances. Error metrics are provided in the lower right.

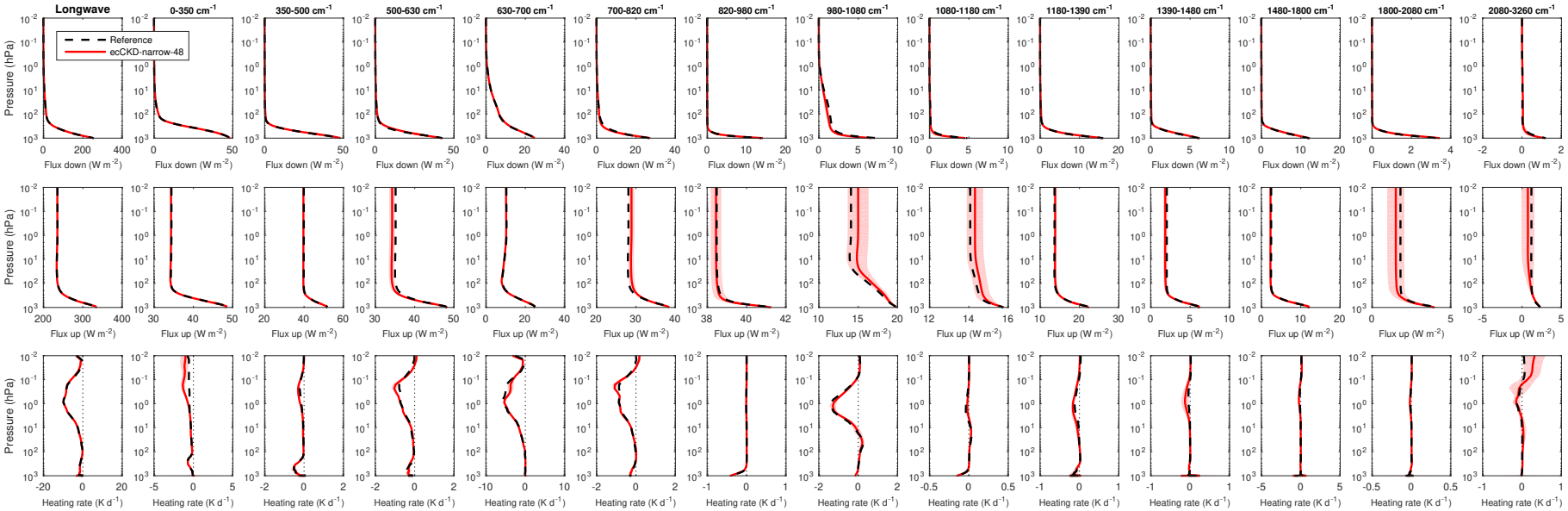

Evaluation of irradiances and heating rates for the broadband (leftmost column of panels) and the 13 narrow longwave bands (other panels) of the global-nwp-narrow-48 CKD model. The black dashed and red solid lines correspond to the average of the 50 profiles for the "present-day" scenario, while the shaded regions encompass 95% of the error.

Model 17: ecCKD global-nwp-narrow-69

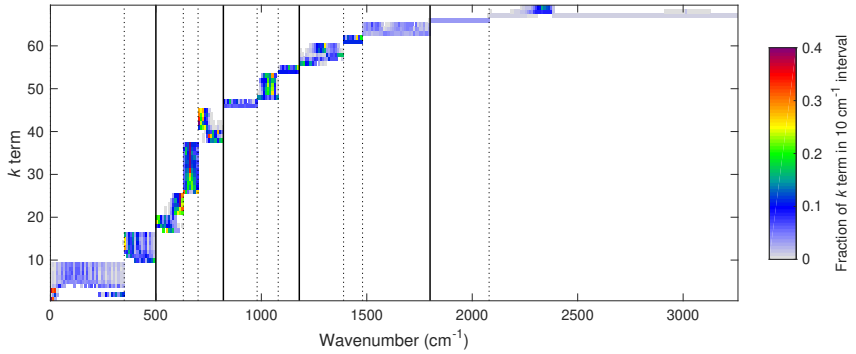

Illustration of the parts of the longwave spectrum that contribute to each k term of the global-nwp-narrow-69 model.

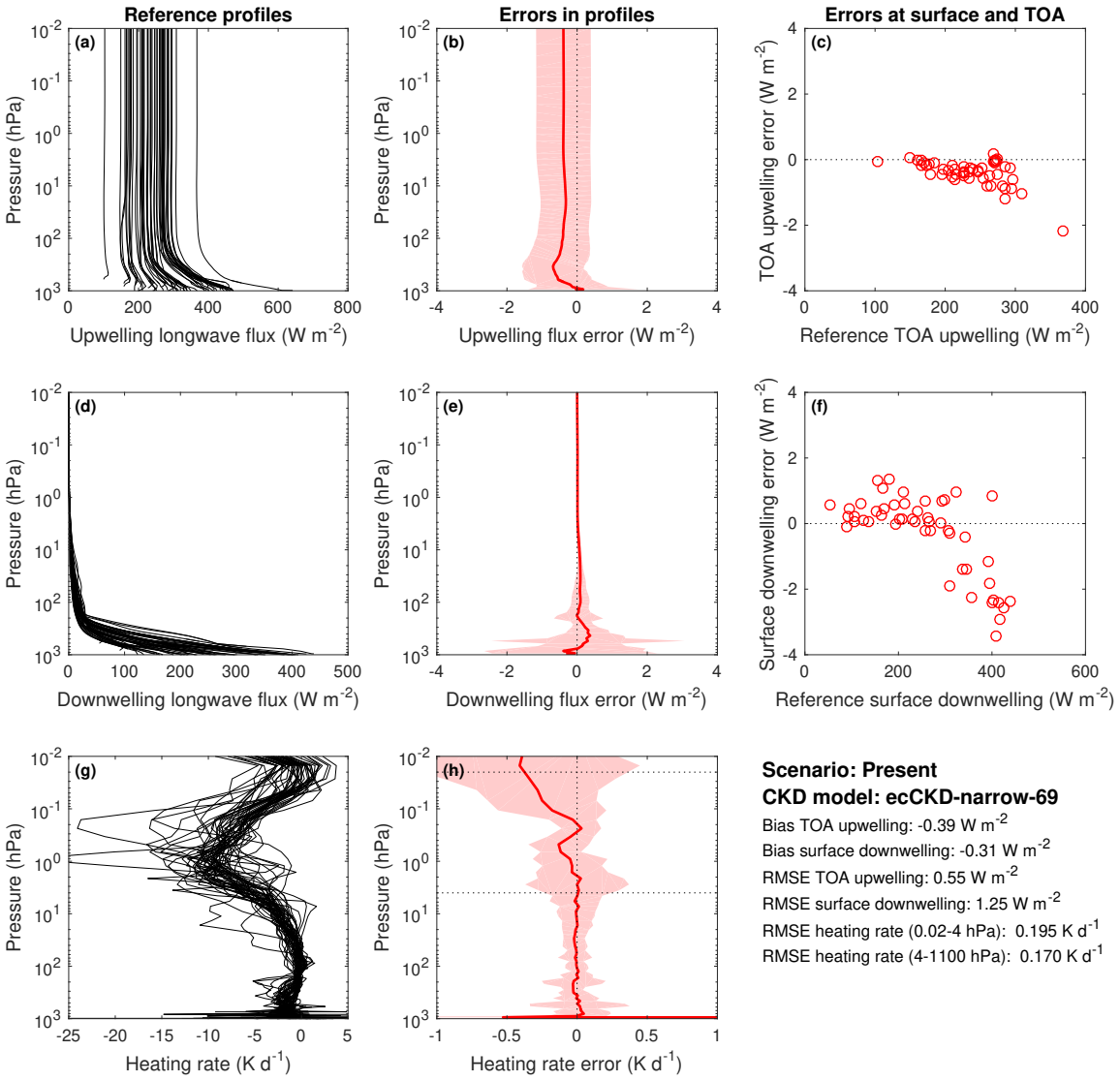

Evaluation of the global-nwp-narrow-69 CKD model for the "present-day" CKDMIP scenario. The left three panels show the irradiances and heating rates from the reference line-by-line calculations. The red lines in the middle three panels show the corresponding bias in these quantities from the CKD model. The shaded regions encompass 95% of the instantaneous errors. Panels c and f depict instantaneous errors in upwelling TOA and downwelling surface irradiances. Error metrics are provided in the lower right.

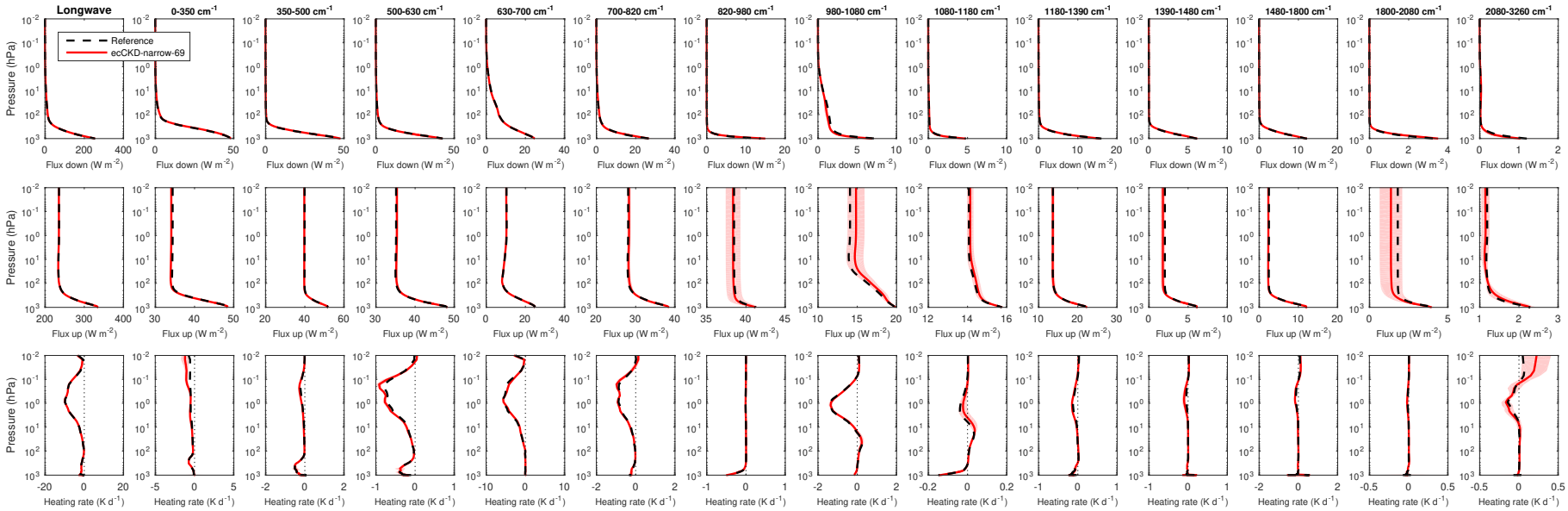

Evaluation of irradiances and heating rates for the broadband (leftmost column of panels) and the 13 narrow longwave bands (other panels) of the global-nwp-narrow-69 CKD model. The black dashed and red solid lines correspond to the average of the 50 profiles for the "present-day" scenario, while the shaded regions encompass 95% of the error.

Model 18: ecCKD global-nwp-narrow-93

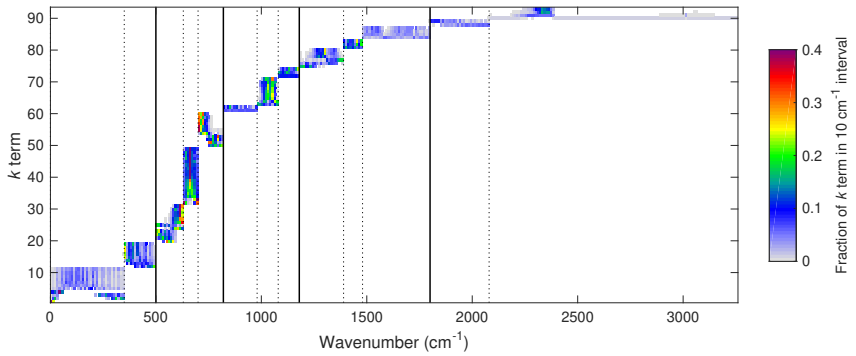

Illustration of the parts of the longwave spectrum that contribute to each k term of the global-nwp-narrow-93 model.

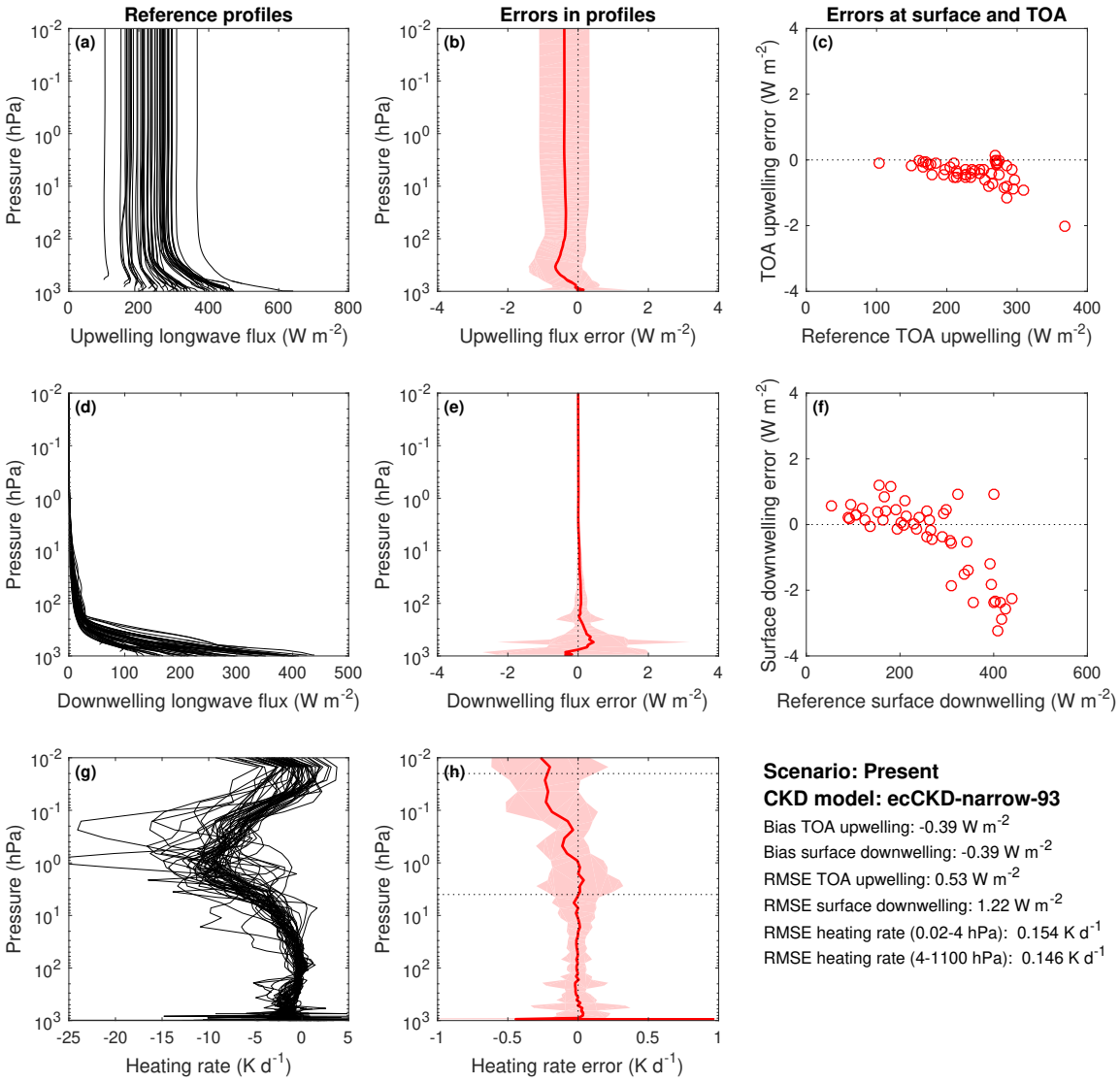

Evaluation of the global-nwp-narrow-93 CKD model for the "present-day" CKDMIP scenario. The left three panels show the irradiances and heating rates from the reference line-by-line calculations. The red lines in the middle three panels show the corresponding bias in these quantities from the CKD model. The shaded regions encompass 95% of the instantaneous errors. Panels c and f depict instantaneous errors in upwelling TOA and downwelling surface irradiances. Error metrics are provided in the lower right.

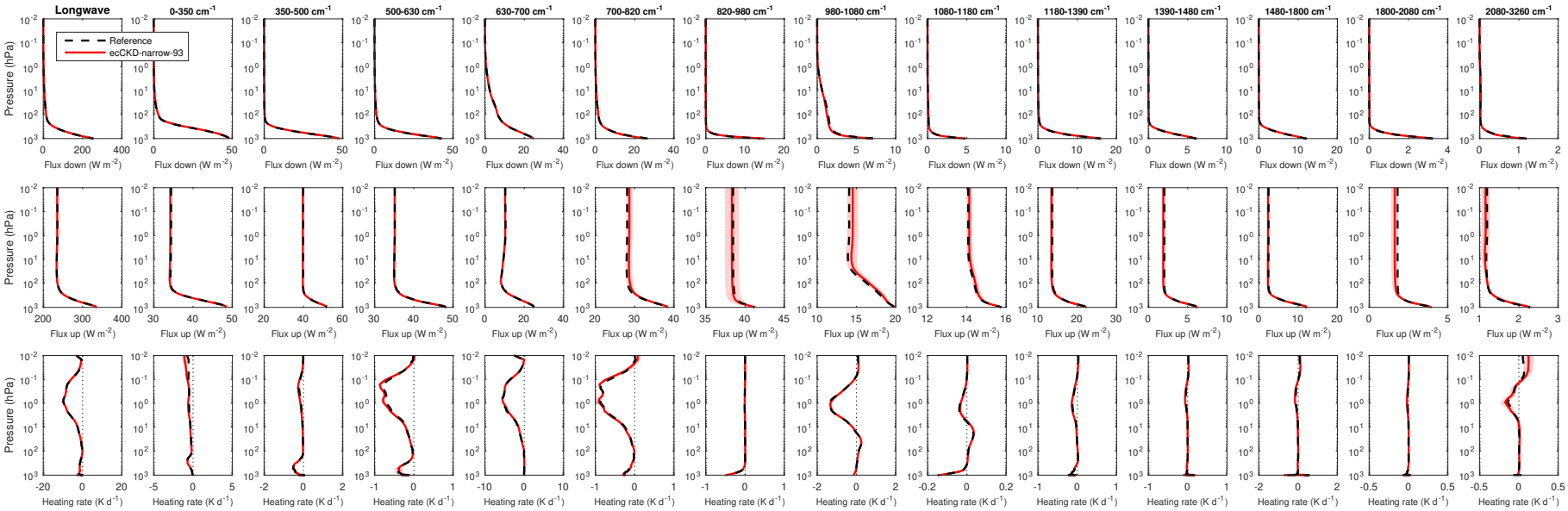

Evaluation of irradiances and heating rates for the broadband (leftmost column of panels) and the 13 narrow longwave bands (other panels) of the global-nwp-narrow-93 CKD model. The black dashed and red solid lines correspond to the average of the 50 profiles for the "present-day" scenario, while the shaded regions encompass 95% of the error.